

Comparison of a Thermopile Broadband Detector and a Photon Detector for the Measurement of Solar Radiation

Part I: Analysis of Simultaneous Data
Part II: Cosine Response Functions

By

Maria Silva Dias, John Davis and Stephen Cox

Department of Atmospheric Science
Colorado State University
Fort Collins, Colorado

March 1976

Colorado
State
University

Department of
Atmospheric Science

Paper No. 250

COMPARISON OF A THERMOPILE BROADBAND DETECTOR
AND A PHOTON DETECTOR FOR THE
MEASUREMENT OF SOLAR RADIATION

Part I. Analysis of Simultaneous Data

Part II. Cosine Response Functions

By

Maria Silva Dias*

John Davis

Stephen Cox

Department of Atmospheric Science

Colorado State University

Fort Collins, Colorado

80523

March 1976

*On leave from University of São Paulo, sponsored by a "Conselho Nacional de Desenvolvimento Científico e Tecnológico (CNPq)" program, Rio de Janeiro, Brazil.

ABSTRACT

Solar radiation instruments manufactured by Eppley Laboratories and Lambda Instruments are compared. The primary method of comparison was a detailed inspection of data collected simultaneously from each of the instruments during the summer and autumn of 1975 at Fort Collins, Colorado. Data were stratified both as a function of sky cover and solar zenith angle. In general, hourly and daily insolation values from the two sets of instruments were within 2.5% of one another.

Deterioration of the nearly linear relationship between the two instruments occurred at large zenith angles. Results of the investigation of the cosine response of the two pyranometers are presented. The Eppley instrument is characterized by undercorrection for large zenith angles while the Lambda instruments device overcorrects. The cosine response characteristics are shown to be consistent with the solar-altitude-dependent regression model.

TABLE OF CONTENTS

PART I

	<u>PAGE</u>
1.1 INTRODUCTION	1
1.2 CHARACTERISTICS OF THE INSTRUMENTS	1
1.3 METHOD OF COMPARISON	5
1.4 DATA	6
1.5 RESULTS	9
1.6 CONCLUSIONS	18

PART II.

2.1 INTRODUCTION	21
2.2 TEST OF THE EPPLEY PYRANOMETER	22
2.3 INTERPRETATION OF DATA AND NOTATION	25
2.4 TEST OF THE LAMBDA PYRANOMETER	32
2.5 SOURCES OF ERROR	37
2.6 CORRECTED COSINE RESPONSE	39
2.7 COMPARISON OF COSINE RESPONSE WITH REGRESSION MODEL	41
2.8 CONCLUSION	44
3.0 REFERENCES	45
ACKNOWLEDGEMENTS	45

LIST OF FIGURES

PART I.

<u>FIGURE</u>		<u>PAGE</u>
1	Spectral response of the pyranometer LI-190SR.	2
2	Spectral response of the pyranometer LI-200SR.	3
3	Eppley Precision Spectral Pyranometer.	4
4	External features of Lambda LI-190SR quantum sensor. The Lambda LI-200SR pyranometer sensor is identical in physical appearance.	7

PART II.

1	Platform used in the cosine response tests.	23
2	Position of the test site with respect to ground objects.	26
3	Azimuthal response of the Eppley pyranometer for zenith angles of 80° , 70° , and 60° .	27
4	Azimuthal response of the Eppley pyranometer for zenith angles of 50° , 40° , and 30° .	28
5	Azimuthal response of the Eppley pyranometer for zenith angles of 20° and 10° .	29
6	Cosine response of the Eppley pyranometer.	31
7	Azimuthal response of the Lambda pyranometer for zenith angles 80° , 70° , and 60° .	33
8	Azimuthal response of the Lambda pyranometer for zenith angles of 50° , 40° , and 30° .	34
9	Azimuthal response of the Lambda pyranometer for zenith angles of 20° , 10° , and 0° .	35
10	Cosine response of the Lambda pyranometer.	36
11	Corrected cosine response of the Eppley pyranometer.	40
12	Corrected cosine response of the Lambda pyranometer.	40
13	Comparison of cosine response data to regression generated data.	43

LIST OF TABLES

PART I.

	<u>PAGE</u>
Table 1. Linear regression parameters for x =Lambda-Visible and y =Eppley-Total.	10
Table 2. Linear regression parameters for x =Lambda-Total and y =Eppley-Total.	10
Table 3. Mean and standard deviation of the hourly and daily errors (*). Lambda-Visible. Sept. 13 to 23. Type of day dependent method.	12
Table 4. Mean and standard deviation of the hourly and daily errors (*). Lambda-Total. Sept. 13 to 23. Type of day dependent method.	12
Table 5. Solar altitude angle as a function of the declination of the sun δ , the equation of time and local standard time for a fixed latitude (38°) and longitude (105°).	14
Table 6. Linear regression parameters for x =Lambda-Visible and y =Eppley-Total.	15
Table 7. Linear regression parameters for x =Lambda-Total and y =Eppley-Total	15
Table 8. Mean and standard deviation of the hourly and daily errors (*) Lambda-Visible. Sept. 13 to 23. Altitude of the sun dependent.	17
Table 9. Mean and standard deviation of the hourly and daily errors (*) Lambda-Total. Sept. 13 to 23. Altitude of the sun dependent.	17

ANALYSIS OF SIMULTANEOUS DATA

PART I.

1.1 - Introduction

Many agriculture-meteorological stations use the Lambda pyranometer in order to measure the solar radiation. The Lambda instruments most commonly used are the pyranometer LI - 190SR and LI - 200 SR which have spectral responses from 0.40 μm to 0.70 μm (Fig. 1) and from 0.40 μm to 1.00 μm (Fig. 2), respectively. The Eppley precision spectral pyranometer measures solar radiation over the range 0.285 μm to 2.800 μm and is appropriate for some meteorological purposes. The relative sensitivity of the Eppley instrument is quite constant and remains between .98 and 1.0 over the .285 μm to 2.800 μm bandpass.

The primary objective of this research is to compare the hourly and daily integrals of downward solar irradiance measured by an Eppley pyranometer with those measured by the Lambda instruments. This comparison will be made by using a regression analysis scheme in which the measurement deduced from the Eppley instrument will be predicted from the Lambda instrument measurement.

1.2 - Characteristics of the Instruments

The Eppley Precision Spectral Pyranometer (Eppley-Total) is an improved smaller model of an earlier instrument introduced in 1957. It comprises a circular, multi-junction, wirewound thermopile immersed beneath two concentric quartz hemispheres. The instrument is discussed in more detail by Robinson et al (1966). A photograph of the Eppley instrument is shown in Fig. 3.

The LI - 190SR quantum sensor (Lambda-Visible) is designed to measure the number of photons in the visible range, received on a plane surface. The silicon photocell sensor response corresponds approximately to the

RELATIVE SPECTRAL RESPONSE

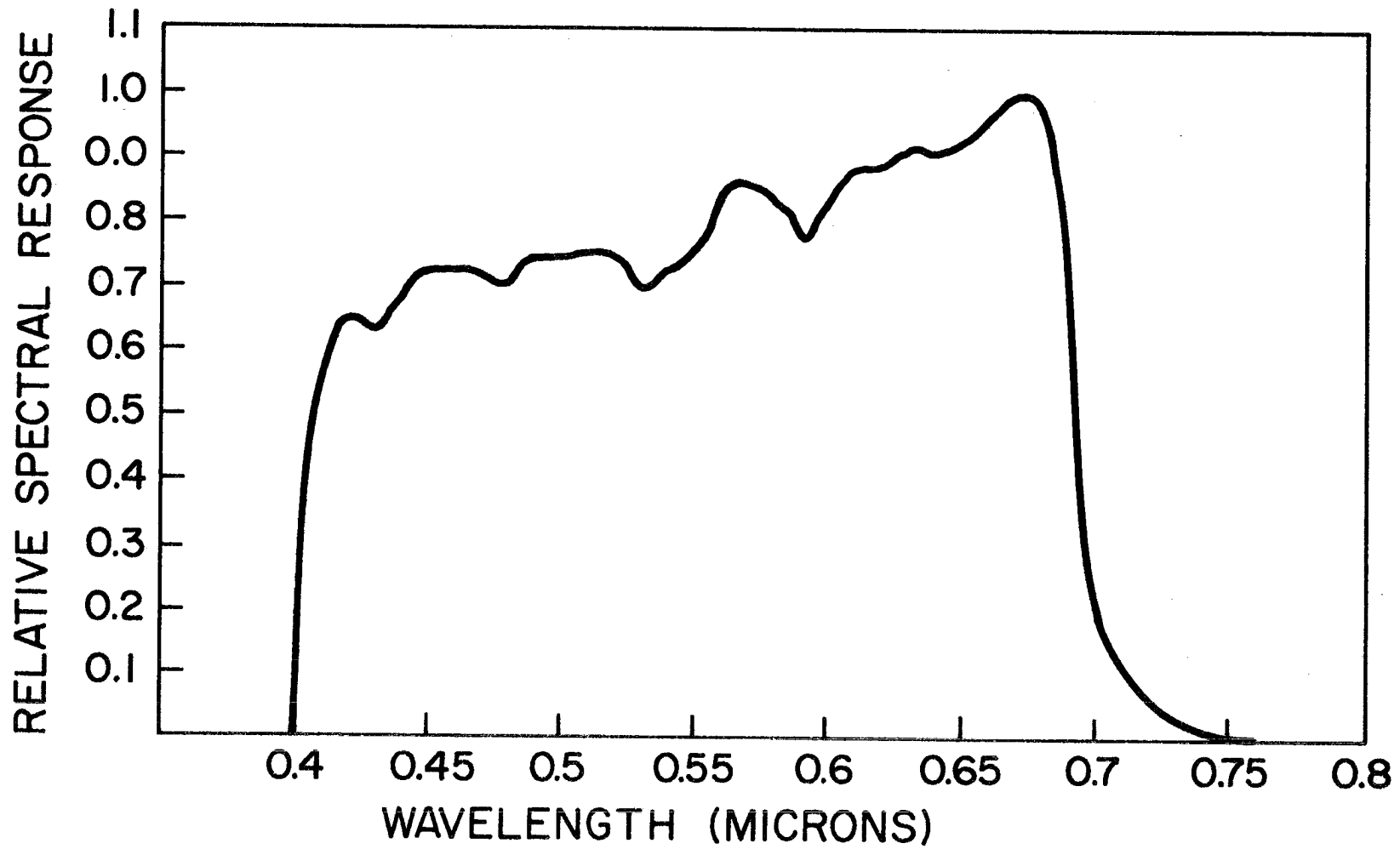


Fig. 1 Spectral response of the Lambda pyranometer LI-190SR

RELATIVE SPECTRAL RESPONSE CURVE

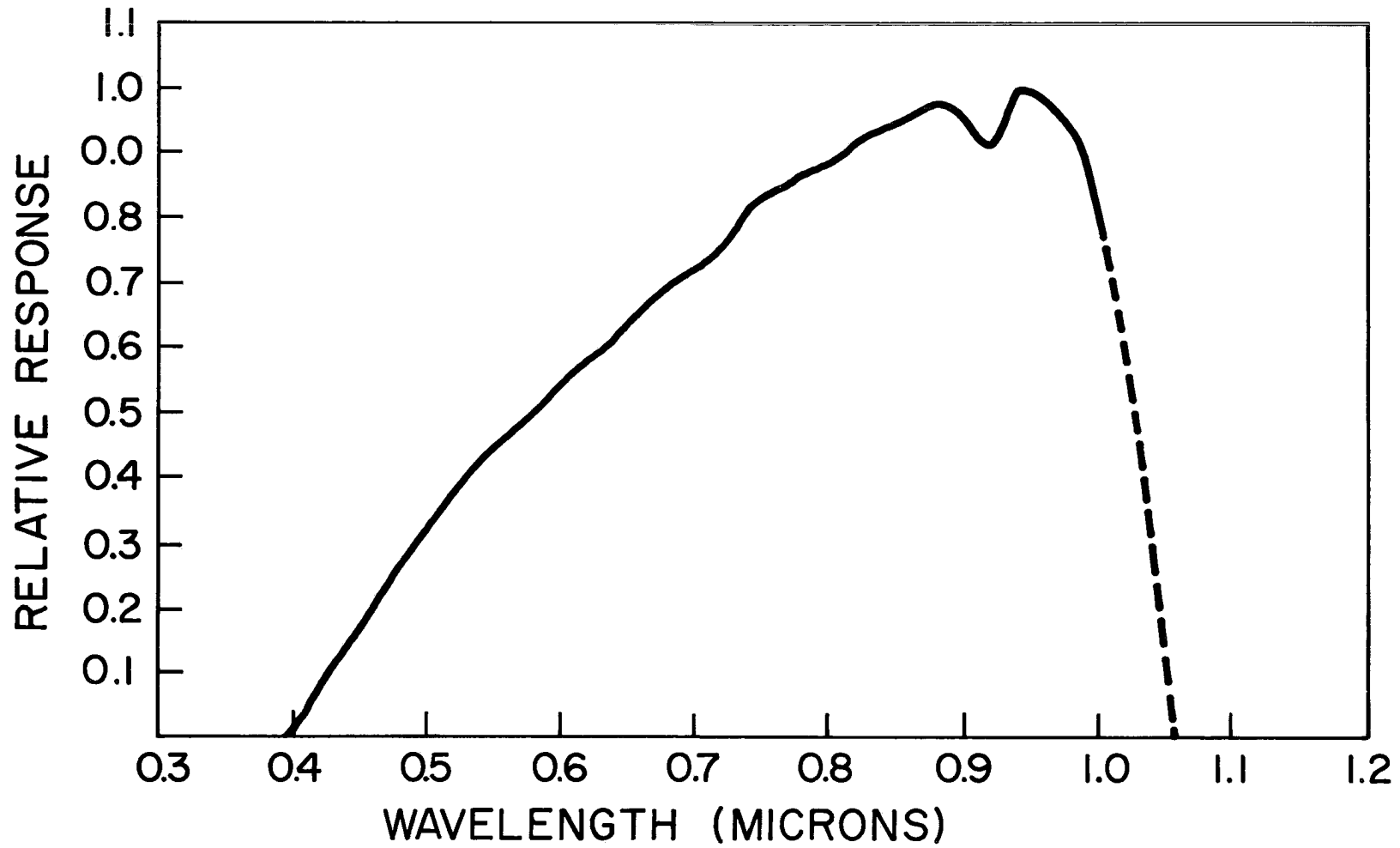


Fig. 2 Spectral response of the Lambda pyranometer LI-200SR



FIGURE 3 - Eppley Precision Spectral Pyranometer.

photosynthetic response of plants (Fig. 4).

The pyranometer sensor LI - 200SR (Lambda-Total) also utilizes a silicon cell. This cell is stable, its response is linear and its temperature sensitivity is low (Fig. 4).

Technical characteristics of the three instruments as given by the respective manufacturers are listed below:

	Lambda-Visible	Lambda-Total	Eppley-Total
1) Range in which radiation is measured	.40 μm - .70 μm	.40 μm - 1.0 μm	.285 μm - 2.8 μm
2) Peak absolute sensitivity	.02mV/W \cdot m ⁻² at .67 μm	.013mV/W \cdot m ⁻² at .94 μm	.007mV/W \cdot m ⁻²
3) Uncertainty in calibration	\pm 4%	\pm 5%	Reproduces the International Pyrheliometric Scale
4) Resistance	604 ohms	100 ohms	300 ohms

1.3 - Method of Comparison

The theory of linear least squares allows one to estimate the parameters a_0 and a_1 in the expression

$$y = a_0 + a_1 x \quad (1)$$

from data consisting of simultaneous measurements of the dependent variable y and the independent variable x . The estimated parameters may be substituted in (1) which may then be used to predict the dependent variable x .

In this case, the two parameters a_0 and a_1 are given by:

$$a_1 = \frac{\sum_{i=1}^N x_i y_i - \left(\sum_{i=1}^N x_i \right) \left(\sum_{i=1}^N y_i \right) / N}{\sum_{i=1}^N x_i^2 - \left(\sum_{i=1}^N x_i \right)^2 / N} \quad (2a)$$

$$a_0 = \frac{1}{N} \left(\sum_{i=1}^N y_i - a_1 \sum_{i=1}^N x_i \right) \quad (2b)$$

where N is the number of simultaneous observations of x and y . A 100 $(1 - \alpha)\%$ confidence interval based on the forecasted value y and on the estimate of the variance s is given by:

$$y \pm t_{N-2} \left(1 - \frac{1}{2} \alpha\right) s \left(1 + \bar{x}'(X'X)^{-1}\bar{x}\right)^{\frac{1}{2}} \quad (3)$$

where $t_{N-2} \left(1 - \frac{1}{2} \alpha\right)$ is the Student's t distribution with $N-2$ degrees of freedom. (3a)

$$s^2 = \frac{1}{N} \left(\sum_{i=1}^N y_i^2 - Na_0^2 - 2a_0a_1 \sum_{i=1}^N x_i - a_1^2 \sum_{i=1}^N x_i^2 \right) \quad (3b)$$

$$(X'X) = \begin{bmatrix} N & \sum_{i=1}^N x_i \\ \sum_{i=1}^N x_i & \sum_{i=1}^N x_i^2 \end{bmatrix} \quad (3c)$$

$(X'X)^{-1}$ is the inverse matrix of $(X'X)$. (3d)

$$\bar{x} = \begin{bmatrix} 1 \\ x \end{bmatrix} \quad (3e)$$

\bar{x}' is the transpose of \bar{x} (3f)

For further reference see Jenkins & Watts 1968 (pp. 132-139).

The Lambda data will be associated with the independent variable x and the Eppley data with the dependent variable y .

1. 4 - Data

All the data used in this research were taken on the roof of the Atmospheric Science Building at Fort Collins, Colorado.

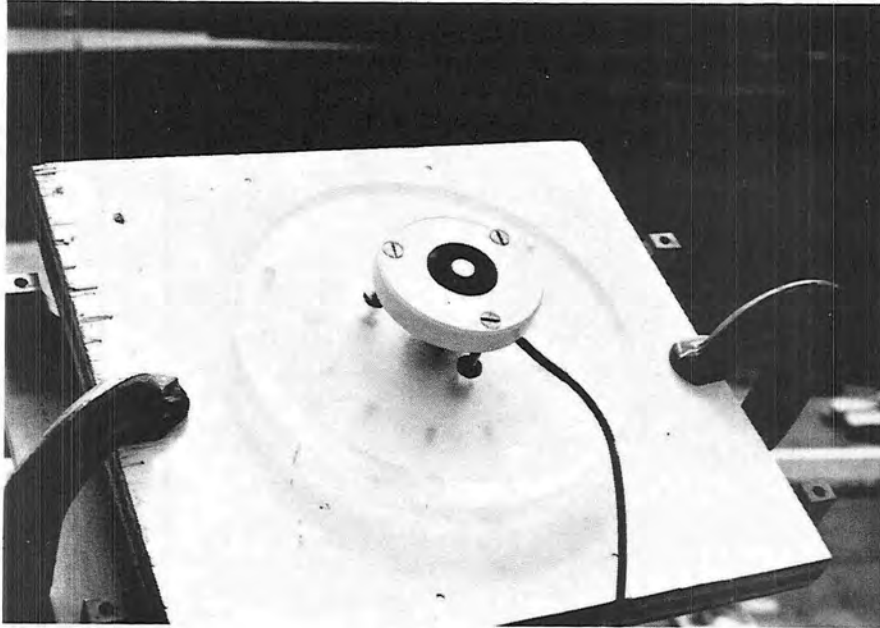


Fig. 4 External features of Lambda LI-190SR quantum sensor.
The Lambda LI-200SR pyranometer sensor is identical
in physical appearance.

The period under consideration is from May 24th to July 15, 1975. If, for any reason, an hourly reading was missing the whole day was disregarded. The complete days were separated into three different classes: overcast, variable and clear. The criterion for such classification is based upon the Lambda pyranometer daily integral (DI). In the Lambda-Visible case the limits are:

$$\begin{aligned} \text{Overcast:} & \quad \text{DI} \leq 3.8 \times 10^7 \mu\text{E.m}^{-2}.\text{day}^{-1} \\ \text{Variable:} & \quad 3.8 \times 10^7 \mu\text{E.m}^{-2}.\text{day}^{-1} < \text{DI} \leq 5.4 \times 10^7 \mu\text{E.m}^{-2}.\text{day}^{-1} \\ \text{Clear:} & \quad 5.4 \times 10^7 \mu\text{E.m}^{-2}.\text{day}^{-1} < \text{DI} \end{aligned}$$

$$\text{where } 1 \mu\text{Einstein} = \frac{\lambda}{6.02 \times 10^{17} h c} \text{Joule}$$

λ is a wavelength, h is Plank's constant and c is the speed of light.

Accordingly, the limits for the Lambda-Total are:

$$\begin{aligned} \text{Overcast:} & \quad \text{DI} \leq 1.8 \times 10^7 \text{J.m}^{-2}.\text{day}^{-1} \\ \text{Variable:} & \quad 1.8 \times 10^7 \text{J.m}^{-2}.\text{day}^{-1} < \text{DI} \leq 2.7 \times 10^7 \text{J.m}^{-2}.\text{day}^{-1} \\ \text{Clear:} & \quad 2.7 \times 10^7 \text{J.m}^{-2}.\text{day}^{-1} < \text{DI} \end{aligned}$$

Corresponding to this classification, the days in each category are:

- a) Lambda-Visible
- Overcast: May 25, 28, 29
June 8, 9, 10, 17
July 9, 14
- Variable: May 27, 30
June 4, 6, 7, 12, 21, 22, 25, 28
July 1, 3, 5, 10, 15
- Clear: May 24, 26
June 1, 2, 5, 11, 13, 20, 23, 24, 26,
27, 29, 30
July 4, 6, 11, 12, 13
- b) Lambda-Total
- Unfortunately in this case it was not possible to use the complete set of days due to some gaps in the Lambda-Total data series. Missing days are:
July 3, 4, 6, 9, 10, 11, 12, 13, 14, 15.

In order to check the method, an independent set of observations were obtained from the period September 13 to 23 (11 days). In this new sample, there were no missing days.

1.5 - Results

In agreement with the classification defined in the preceding section, the linear least squares regression method was applied to each category in order to determine the parameters a_0 and a_1 in Eq. (1) for overcast, variable and clear conditions. Consequently, the number of simultaneous observations is the number of days in each category times 18 hourly readings (from 4:00 to 21:00). The parameters of the linear regression are shown in Tables 1 and 2 which also include

$$(X'X)^{-1} = \begin{bmatrix} \sum_{i=1}^N x_i^2 / \text{Det}(X'X) & - \sum_{i=1}^N x_i / \text{Det}(X'X) \\ - \sum_{i=1}^N x_i / \text{Det}(X'X) & N / \text{Det}(X'X) \end{bmatrix} = \begin{bmatrix} a & b \\ c & d \end{bmatrix} \quad (4)$$

the coefficient of correlation r and the residual variance s . Hence, the 95% confidence interval for the forecasted value is given by

$$y \pm 1.96 s (1 + a + (b + c)x + dx^2)^{1/2} \quad (5)$$

In practice, because of the small values of a , b , c and d , the approximate formula for the confidence interval may be used:

$$y \pm 1.96 s \quad (6)$$

The error which results from the approximation is of the order of 0.5%, which is negligible compared to the calibration errors of the Lambda pyranometers.

According to Tables 1 and 2, an increase in the absolute value of a_0 and in the values of a_1 and s occurs as the type of day changes from

TABLE 1 - Linear regression parameters for $x = \text{Lambda-Visible}$ and
 $y = \text{Eppley-Total}$ ** Type of day dependent method

	OVERCAST	VARIABLE	CLEAR
N	162	270	342
$a_0(\text{Joule.m}^{-2})$	-15,958.8	-16,282.2	-28,969.8
$a_1(\text{Joule}/\mu\text{E})$	0.4830	0.4925	0.5021
$s(\text{Joule.m}^{-2})$	29,092.2	41,661.0	49,338.0
a	$.1095 \times 10^{-1}$	$.8249 \times 10^{-2}$	$.7516 \times 10^{-2}$
b	$-.317 \times 10^{-8}$	$-.176 \times 10^{-8}$	$-.138 \times 10^{-8}$
c	$-.317 \times 10^{-8}$	$-.176 \times 10^{-8}$	$-.138 \times 10^{-8}$
d	$.211 \times 10^{-14}$	$.676 \times 10^{-15}$	$.414 \times 10^{-15}$
r	0.99	0.99	0.99

TABLE 2 - Linear regression parameters for $x = \text{Lambda-Total}$ and
 $y = \text{Eppley-Total}$ ** Type of day dependent method

	OVERCAST	VARIABLE	CLEAR
N	126	198	252
$a_0(\text{Joule.m}^{-2})$	-10,510.8	-20,713.8	-22,825.8
$a_1(\text{Joule}/\text{Joule})$	1.0217	1.0285	1.0428
$s(\text{Joule.m}^{-2})$	25,846.2	31,788.0	33,615.0
a	$.1439 \times 10^{-1}$	$.1162 \times 10^{-1}$	$.1024 \times 10^{-1}$
b	$-.101 \times 10^{-7}$	$-.532 \times 10^{-8}$	$-.389 \times 10^{-8}$
c	$-.101 \times 10^{-7}$	$-.532 \times 10^{-8}$	$-.389 \times 10^{-8}$
d	$.157 \times 10^{-13}$	$.431 \times 10^{-14}$	$.242 \times 10^{-14}$
r	0.99	0.99	0.99

overcast to variable and clear. The increase of the residual variance, s , will produce a larger confidence interval for the forecasted value y . In all cases, the coefficient of correlation r is 0.99 showing how closely Eq. (1) fits the experimental data.

The results obtained by the linear regression were applied to the independent set of data September 13 to 23. For each hour the percentage error was computed and an average percentage error and standard deviation interval for the eleven day period were determined. These results are a measure of the degree of fitness of the method, at least during the period under consideration; this may be seen in Tables 3 and 4. The same procedure was also carried out for the daily integrals (last line of Tables 3 and 4).

These tables also show the mean error and the standard deviation interval in absolute units ($\text{Joule}\cdot\text{m}^{-2}\cdot\text{hr}^{-1}$).

While the relative errors in the early morning and late afternoon seem too large, we see that indeed the errors are on the order of $1.2 \times 10^4 \text{ J}\cdot\text{m}^{-2}\cdot\text{hr}^{-1}$ which is not too much when compared with an hourly integral at 12:00 (about $2.4 \times 10^6 \text{ J}\cdot\text{m}^{-2}\cdot\text{hr}^{-1}$).

The daily integrals are very close to the Eppley value for it, especially in the case of the forecasted value based on the Lambda-Visible sensor. The mean error in this case is $2.46 \times 10^5 \text{ J}\cdot\text{m}^{-2}\cdot\text{day}^{-1}$ with a standard deviation of $1.8 \times 10^5 \text{ J}\cdot\text{m}^{-2}\cdot\text{day}^{-1}$. (The reader should refer to section 1.4 for the order of magnitude of the daily integrals in $\text{J}\cdot\text{m}^{-2}\cdot\text{day}^{-1}$.)

Another way to organize the data for determining the coefficients of linear regression is to consider the parameters a_0 and a_1 as a function of the altitude angle of the sun, disregarding the effect of cloud cover. The procedure to be followed in this case is:

TABLE 3 - Mean and standard deviation of the hourly and daily errors(*).

Lambda-Visible. Sept. 13 to 23. Type of day dependent method.

Hour	Mean($\text{J.m}^{-2}.\text{hr}^{-1}$)	S.D.($\text{J.m}^{-2}.\text{hr}^{-1}$)	Mean(%)	S.D.(%)
4	-----	-----	-----	-----
5	11354.4	3620.4	97.30	5.80
6	-1511.4	15255.6	-0.38	4.55
7	-11702.4	18305.4	-1.25	1.91
8	-2412.6	23290.2	-0.16	1.35
9	2468.4	18516.6	0.11	0.82
10	21198.0	25247.4	0.85	0.96
11	31321.8	35078.4	1.12	1.37
12	43747.8	42395.4	1.47	1.73
13	35402.4	26678.4	1.35	1.50
14	37678.8	28563.6	1.94	1.15
15	35970.6	13635.0	2.83	1.00
16	24712.2	17655.0	4.25	3.42
17	10483.2	9869.4	10.56	18.98
18	-----	-----	-----	-----
Daily Value	$2.458 \times 10^5 \text{ J.m}^{-2}.\text{day}^{-1}$	$1.836 \times 10^5 \text{ J.m}^{-2}.\text{day}^{-1}$	1.35%	.87%

TABLE 4 - Mean and standard deviation of the hourly and daily errors (*).

Lambda-Total. Sept. 13 to 23. Type of day dependent method.

Hour	Mean($\text{J.m}^{-2}.\text{hr}^{-1}$)	S.D.($\text{J.m}^{-2}.\text{hr}^{-1}$)	Mean(%)	S.D.(%)
4	-----	-----	-----	-----
5	11284.8	2949.0	97.54	5.58
6	3692.4	13857.0	0.25	3.84
7	6805.8	13920.6	0.81	1.60
8	17227.2	8869.2	1.03	0.53
9	25071.6	18564.6	1.05	0.94
10	44668.8	30895.8	1.73	1.29
11	59585.4	58177.8	2.28	1.19
12	68689.8	44748.6	2.76	1.13
13	52917.6	29336.4	2.45	0.73
14	44415.0	27532.2	2.45	0.85
15	36310.8	33372.0	2.66	1.93
16	31382.4	10502.4	7.05	6.35
17	22479.6	12978.6	21.02	27.65
18	-----	-----	-----	-----
Daily Value	$4.303 \times 10^5 \text{ J.m}^{-2}.\text{day}^{-1}$	$1.933 \times 10^5 \text{ J.m}^{-2}.\text{day}^{-1}$	2.28%	0.65%

(*) Error = $y_{\text{observed}} - y_{\text{forecasted}}$

- a) Determine the solar altitude angle (SAA) intervals with the corresponding regression parameters.
- b) Given an hour interval, compute the SAA average value.
- c) Associate the SAA average value with the appropriate SAA interval among those calculated in step a).
- d) Determine the corresponding parameters a_0 and a_1 to forecast the Eppley hourly readings.

The variation of solar altitude during the period May 29 to July 13 is shown in Table 5. As may be seen from that table, the symmetric hours around noon were put together in order to calculate the mean SAA for each two symmetric hours. This arrangement defines eight SAA intervals; these intervals are listed below:

	11	\leq	2.87°
2.87°	<	12	\leq 13.78°
13.78°	<	13	\leq 25.24°
25.24°	<	14	\leq 36.96°
36.96°	<	15	\leq 48.77°
48.77°	<	16	\leq 60.16°
60.16°	<	17	\leq 70.06°
70.06°	<	18	

The method was applied to the whole set of data in each two symmetric hours. As a result, eight sets of parameters corresponding to the eight SAA intervals defined above were defined and are shown in Tables 6 and 7. The parameters a_1 and s increase as SAA varies from low to higher values; a_0 , on the other hand, initially shows an increase and then a sharp decrease takes place. The correlation coefficient, r , shows slightly smaller values for the first SAA interval. This is probably due to

TABLE 5 - Solar altitude angle as a function of the declination of the sun δ , the equation of time and local standard time (as given by the Smithsonian Meteorological Tables) for a fixed latitude (38°) and longitude (105°).

Day	δ	eq.t.	4:00	5:00	6:00	7:00	8:00	9:00	10:00	11:00	12:00	13:00	14:00	15:00	16:00	17:00	18:00	19:00	20:00
29/5	21 31'	2m51s	-7.64	2.56	13.58	25.10	36.88	48.63	59.89	69.41	73.49	68.66	58.87	47.53	35.75	23.99	12.50	1.55	-8.56
1/6	21 57'	2m27s	-7.38	2.78	13.77	25.27	37.04	48.80	60.11	69.73	73.94	69.08	59.22	47.85	36.07	24.31	12.85	1.92	-8.17
5/6	22 28'	1m49s	-7.11	3.00	13.95	25.42	37.18	48.96	60.32	70.07	74.86	69.58	59.66	48.25	36.47	24.72	13.27	2.36	-7.69
9/6	22 52'	1m06s	-6.94	3.13	14.05	25.50	37.25	49.04	60.43	70.30	74.86	70.00	60.03	48.61	36.82	25.07	13.64	2.75	-7.29
13/6	23 10'	0m18s	-6.85	3.19	14.07	25.51	37.25	49.04	60.47	70.43	75.17	70.35	60.36	48.92	37.13	25.39	13.96	3.08	-6.94
17/6	23 22'	-0m33s	-6.84	3.17	14.03	25.45	37.18	48.98	60.43	70.47	75.37	70.62	60.64	49.19	37.40	25.66	14.24	3.36	-6.66
21/6	23 27'	-1m25s	-6.91	3.07	13.92	25.33	37.06	48.85	60.32	70.41	75.45	70.81	60.84	49.41	37.61	25.88	14.45	3.57	-6.46
25/6	23 25'	-2m17s	-7.07	2.90	13.74	25.14	36.87	48.67	60.14	70.26	75.41	70.90	60.98	49.56	37.77	26.03	14.59	3.70	-6.35
29/6	23 17'	-3m07s	-7.30	2.67	13.50	24.91	36.64	48.43	59.91	70.04	75.27	70.91	61.05	49.65	37.86	26.12	14.67	3.76	-6.32
1/7	23 10'	-3m31s	-7.45	2.52	13.36	24.77	36.50	48.29	59.77	69.89	75.15	70.87	61.06	49.67	37.88	26.13	14.67	3.75	-6.34
5/7	22 52'	-4m16s	-7.78	2.19	13.05	24.46	36.19	47.99	59.45	69.55	74.84	70.73	61.01	49.65	37.87	26.12	14.64	3.69	-6.43
9/7	22 28'	-4m56s	-8.18	1.82	12.69	24.11	35.85	47.65	59.09	69.14	74.43	70.49	60.88	49.57	37.80	26.03	14.53	3.55	-6.61
13/7	21 57'	-5m30s	-8.65	1.38	12.27	23.72	35.47	47.26	58.67	68.65	73.91	70.13	60.66	49.39	37.64	25.86	14.34	3.32	-6.89

Mean solar altitude angle for the hours:

4:00	5:00	6:00	7:00	8:00	9:00	10:00	11:00	12:00
20:00	19:00	18:00	17:00	16:00	15:00	14:00	13:00	
-7.19	2.87	13.78	25.24	36.96	48.77	60.16	70.06	74.75

TABLE 6 - Linear regression parameters for x = Lambda-Visible and y = Eppley-Total, Altitude of the sun dependent method. (N = 86)

SAA interval	a_0 ($J \cdot m^{-2}$)	a_1 ($J/\mu E$)	s ($J \cdot m^{-2}$)	a	b	c	d	r
11	-789.0	0.4448	4724.4	$.3532 \times 10^{-1}$	$-.773 \times 10^{-6}$	$-.773 \times 10^{-6}$	$.252 \times 10^{-10}$	0.90
12	4593.0	0.4537	15969.6	$.5948 \times 10^{-1}$	$-.869 \times 10^{-7}$	$-.869 \times 10^{-7}$	$.158 \times 10^{-12}$	0.99
13	1722.0	0.4688	26439.0	$.7131 \times 10^{-1}$	$-.382 \times 10^{-7}$	$-.382 \times 10^{-7}$	$.244 \times 10^{-13}$	0.99
14	-16142.4	0.4865	38584.2	$.9070 \times 10^{-1}$	$-.283 \times 10^{-7}$	$-.283 \times 10^{-7}$	$.101 \times 10^{-13}$	0.99
15	-41226.0	0.4955	45449.4	$.8640 \times 10^{-1}$	$-.198 \times 10^{-7}$	$-.198 \times 10^{-7}$	$.527 \times 10^{-14}$	0.99
16	-58365.6	0.5017	52285.2	$.8401 \times 10^{-1}$	$-.156 \times 10^{-7}$	$-.156 \times 10^{-7}$	$.335 \times 10^{-14}$	0.99
17	-87996.6	0.5117	54293.4	$.9783 \times 10^{-1}$	$-.165 \times 10^{-7}$	$-.165 \times 10^{-7}$	$.318 \times 10^{-14}$	0.99
18	-111687.0	0.5167	57972.6	.1075	$-.171 \times 10^{-7}$	$-.171 \times 10^{-7}$	$.304 \times 10^{-14}$	0.99

TABLE 7 - Linear regression parameters for x = Lambda-Total and y = Eppley-Total. Altitude of the sun dependent method. (N = 64)

SAA interval	a_0 ($J \cdot m^{-2}$)	a_1 (J/J)	s ($J \cdot m^{-2}$)	a	b	c	d	r
11	5578.2	0.4788	6996.6	$.3248 \times 10^{-1}$	$-.880 \times 10^{-6}$	$-.880 \times 10^{-6}$	$.460 \times 10^{-11}$	0.78
12	5391.6	0.9436	15539.4	$.7884 \times 10^{-1}$	$-.233 \times 10^{-6}$	$-.233 \times 10^{-6}$	$.858 \times 10^{-12}$	0.99
13	6492.0	0.9834	24234.6	$.9082 \times 10^{-1}$	$-.101 \times 10^{-7}$	$-.101 \times 10^{-7}$	$.135 \times 10^{-13}$	0.99
14	3051.6	1.0096	29532.0	.1284	$-.826 \times 10^{-7}$	$-.826 \times 10^{-7}$	$.605 \times 10^{-13}$	0.99
15	-30427.8	1.0361	30814.2	.1125	$-.539 \times 10^{-7}$	$-.539 \times 10^{-7}$	$.300 \times 10^{-13}$	0.99
16	-52710.6	1.0462	35597.4	.1008	$-.394 \times 10^{-7}$	$-.394 \times 10^{-7}$	$.181 \times 10^{-13}$	0.99
17	-78753.0	1.0621	35129.4	.1205	$-.433 \times 10^{-7}$	$-.433 \times 10^{-7}$	$.179 \times 10^{-13}$	0.99
18	-82355.4	1.0639	38595.4	.1272	$-.424 \times 10^{-7}$	$-.424 \times 10^{-7}$	$.161 \times 10^{-13}$	0.99

differences in the cosine response of the Lambda and Eppley instruments. Obviously, if the differences were systematic, the linear regression method would take it into account, giving a higher correlation coefficient. For the other intervals, the value of r is 0.99.

Step b) is carried out by computing the SAA average value during one hour interval by the formula:

$$\bar{A} = \frac{1}{h_2 - h_1} \int_{h_1}^{h_2} \text{arc sin} (\sin \phi \sin \delta + \cos \phi \cos \delta \cos h) dh$$

where ϕ is the latitude, δ is the declination of the sun for the day under consideration (see Table 169 - Smithsonian Meteorological Tables) and h is the hour angle given by

$$h = 180^\circ - 15. \quad (\text{true solar time})$$

(see Smithsonian Meteorological Tables, page 497, for conversion from local standard time to true solar time).

Steps b), c), and d) were applied to the sample September 13 to 23 leading to Tables 8 and 9 which were constructed in the same way as Tables 3 and 4. Again, these tables show mean errors in absolute and relative units. The fitting to the Eppley readings seems to be better in the SAA dependent model than in the type of day dependent model. At least for early morning, later afternoon and daily integrals, the predicted values are closer to the Eppley values than in the first model.

As shown by Tables 3, 4, 8 and 9, the errors have a tendency to increase during the afternoon period. A plausible hypothesis is that the nearby mountains west of the instrument location affect the solar irradiance by the azimuthal solar angle variation during the year. For a fixed low altitude, the sun may be behind the mountains during the

TABLE 8 - Mean and standard deviation of the hourly and daily errors. (*)
 Lambda-Visible. Sept. 13 to 23. Altitude of the sun dependent.

Hour	Mean($J.m^{-2}.hr^{-1}$)	S.D.($J.m^{-2}.hr^{-1}$)	Mean(%)	S.D.(%)
4	----	----	----	----
5	-8.4	2917.8	-4.10	21.33
5	3211.8	13401.6	0.97	4.05
7	10519.2	18819.6	0.97	2.03
3	3483.0	26266.8	0.17	1.53
9	-4937.4	27552.0	-0.20	1.19
10	6327.0	37457.4	0.15	1.47
11	11733.6	40497.0	0.32	1.15
12	30357.0	43607.4	0.95	1.63
13	37211.4	30705.0	1.96	1.30
14	44592.0	32848.2	2.51	1.17
15	42855.6	24237.0	3.17	1.43
16	33346.8	31471.2	4.14	3.80
17	3042.0	9976.8	0.99	5.12
18	----	----	----	----
Daily Value	$2.213 \times 10^5 J.m^{-2}.day^{-1}$	$2.793 \times 10^5 J.m^{-2}.day^{-1}$	1.05%	1.36%

TABLE 9 - Mean and standard deviation of the hourly and daily errors. (*)
 Lambda-Total. Sept. 13 to 23. Altitude of the sun dependent.

Hour	Mean($J.m^{-2}.hr^{-1}$)	S.D.($J.m^{-2}.hr^{-1}$)	Mean(%)	S.D.(%)
4	----	----	----	----
5	3103.8	2178.0	24.35	10.74
6	9465.6	10546.2	2.88	2.95
7	24679.2	11812.8	2.63	1.46
8	24244.2	8734.2	1.44	0.52
9	16869.0	16918.8	0.70	0.82
10	35871.0	26262.6	1.41	1.10
11	50301.0	26335.2	2.05	0.85
12	62534.4	33658.8	2.80	1.07
13	51620.4	19827.6	3.25	2.49
14	44142.0	20518.8	2.82	0.64
15	37914.0	35432.4	2.63	2.03
16	34455.0	14376.6	6.51	3.43
17	15185.4	10390.2	12.38	14.40
18	----	----	----	----
Daily Value	$3.976 \times 10^5 J.m^{-2}.day^{-1}$	$1.603 \times 10^5 J.m^{-2}.day^{-1}$	2.15%	0.52%

(*) - Error = $y_{observed} - y_{forecasted}$

period September 13 to 23 (azimuth at sunset near 270°) while during May 24 to July 15, due to a smaller azimuthal angle (between 240° and 250°), the instruments may be still registering the direct sunlight. The parameter a_0 is inversely dependent upon the actual magnitude of the solar irradiance (see Table 1 and 2). During the September data sample, at a low SAA, the instruments would be recording diffuse radiation while for the same SAA during May 24 to July 15 the instruments might be recording direct and diffuse radiation. A large absolute value of the irradiance at low SAA during May 24 to July 15 implies an underestimated value of the parameter a_0 under the same SAA conditions, during September.

1.6 - Conclusions

In general, the Lambda-Visible sensor presents a smaller mean error when forecasting the Eppley reading, but more scattered than the Lambda-Total results. The altitude-of-the-sun dependent stratification shows better results during the early morning, late afternoon and daily integral than the type of day stratification. The mean errors in the early morning and late afternoon are of the order of $1.2 \times 10^4 \text{ J}\cdot\text{m}^{-2}\cdot\text{hr}^{-1}$ and may reach $7.2 \times 10^4 \text{ J}\cdot\text{m}^{-2}\cdot\text{hr}^{-1}$ around noon which is not too much if compared to an hourly integral at noon (around $2.4 \times 10^6 \text{ J}\cdot\text{m}^{-2}\cdot\text{hr}^{-1}$). The errors in the daily integral are on the order of $2.4 \times 10^5 \text{ J}\cdot\text{m}^{-2}\cdot\text{hr}^{-1}$ in the case based upon the Lambda-Visible sensor and around $4.2 \times 10^5 \text{ J}\cdot\text{m}^{-2}\cdot\text{hr}^{-1}$ in the case based upon the Lambda-Total series. In both cases, those errors lie between 1% and 2.5% of the value derived from the Eppley data.

The data used in this research were obtained from a high altitude location (approximately 1500 m) with a generally low atmospheric

water vapor content, therefore, the parameters a_0 and a_1 may not be valid for other locations.

The techniques described and applied to the limited data set in this study should be applied to simultaneous observations of the two types of instruments from other locations, especially those representing higher water vapor content.

COSINE RESPONSE FUNCTIONS

PART II

2.1- INTRODUCTION

In the first section of this report it was shown that the total irradiance fields, as measured by an Eppley pyranometer, could be accurately duplicated by applying a linear regression model to data obtained from a Lambda pyranometer. The values obtained for the coefficients in the model result from differences in the responses of the two pyranometers to changing solar and atmospheric parameters. Dependence on one of these parameters, the changing solar angle, is easily examined. The second section of this report compares the cosine response of the radiometers in question. It also shows that the variation of regression coefficients, calculated as a function of solar altitude angle, can be, to some extent, attributed to the difference in the cosine response of the instruments.

The test of the cosine response of a pyranometer is an examination of the instrument's adherence to the relation

$$Q_H = Q_N \cos \theta + q, \quad (1)$$

where Q_H is the incident radiation on a horizontal surface, Q_N is the direct solar radiation on a surface normal to the radiation, θ is the zenith angle and q is the diffuse radiation (Robinson, 1966).

The purpose of this experiment was to compare the cosine response of an Eppley precision spectral pyranometer to that of a Lambda pyranometer. Characteristics of both instruments are described in Part I of this report.

2.2 - TEST OF THE EPPLEY PYRANOMETER

In order to measure the cosine response of the two instruments, a turntable was constructed on a platform so that it could be placed on an equatorial mount. The turntable provided for the taking of several azimuthal readings at each zenith angle. The equatorial mount allowed for variation in the zenith angle from 90° to 0° and provided a stable support for the turntable and radiometer.

Because the sun was used as the source in these experiments, variations in zenith and azimuth due to earth rotation become a factor if the time taken to accomplish the experiment is long. In order to minimize these effects two precautions were taken. First, to minimize the variation in zenith, the time chosen for the experiment was near solar noon. At this time variation in zenith with time is at a minimum. Also, optical path length is a minimum at this time so that effects due to variations in turbidity, water vapor, etc. with time should be minimized. Second, an attempt was made to compensate for changing azimuth by using the equatorial mount in the operational mode. Obviously, such compensation is by no means exact. The apparatus used in the test is shown in Fig. 1 with the Lambda pyranometer in place.

The outputs of the radiometers were amplified by means of an Acromag model 311-BX-U amplifier and the data recorded using Monitor Labs model 9100 data system in conjunction with a Cipher model 85H recorder.

For the actual collection of data, an Eppley pyranometer (serial number 12511F3) was cleaned and mounted on the turntable which was then secured to the equatorial mount using "C" clamps. By adjusting the clamps it was ensured that the plane of the radiometer was parallel to that of the platform on the equatorial mount.

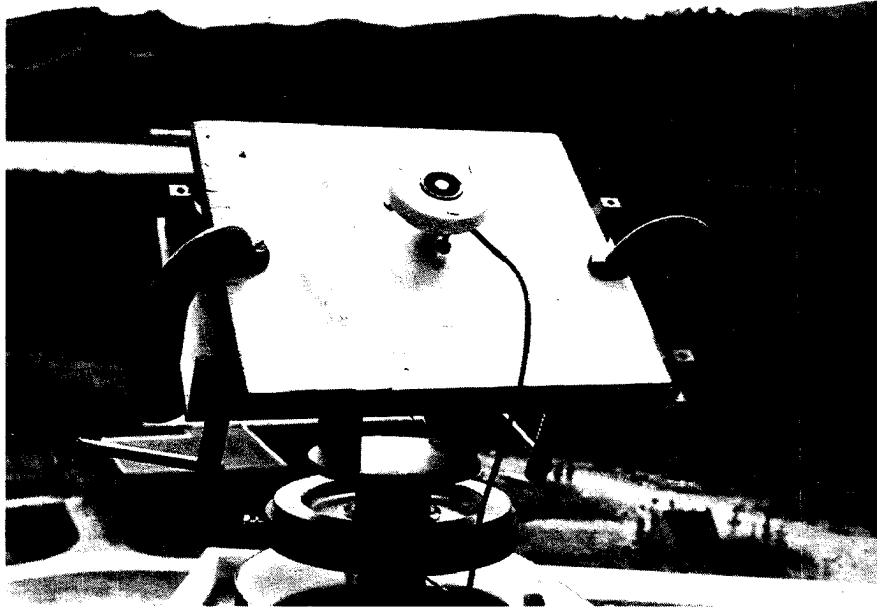


Figure 1. Platform used in the cosine response tests.

Beginning at $\theta = 90^\circ$ (θ is the zenith angle), data was taken for each 30° of azimuth at zenith angles from 90° to 10° . The $\theta = 0^\circ$ data is missing due to a poor electrical connection which invalidated this data. Each azimuthal reading consisted of approximately five data points taken at one second intervals. Consequently, each zenith calculation was based on approximately sixty data points.

2.3 - Interpretation of the Data and Notation

For the interpretation of the data, it was assumed that no direct radiation was incident on the sensor at $\theta = 90^\circ$. Also, it was assumed for the first of these tests that the diffuse component of the radiation was constant throughout the test. This is not the case in reality, however, since the radiometer measures radiation from the ground and ground objects along with some sky radiation for large values of θ , as θ decreases, the amount of ground radiation decreases and the actual sky radiation increases. Figure 2 shows the test site in relation to ground objects. The large radar dome was calculated to have subtended 0.1 steradians of the field of view. The cloudy sky conditions evident in this photograph were not typical of those existing on the test dates.

In order to observe the actual cosine response, the diffuse component (as measured at $\theta = 90^\circ$) was subtracted from each of the data values, thus yielding a "direct component only" value. This is equivalent to setting $q = 0$ in Eq. 1. It is the instrument's response to this component which is under scrutiny. If these values are denoted by $R_\theta, \bar{\phi}$, where θ is the zenith angle and $\bar{\phi}$ indicates an average over all the azimuthal angles ϕ , then true cosine response requires

$$R_{0, \bar{\phi}} = \frac{R_{10, \bar{\phi}}}{\cos 10^\circ} = \frac{R_{20, \bar{\phi}}}{\cos 20^\circ} = \dots = \frac{R_{80, \bar{\phi}}}{\cos 80^\circ} \quad (2)$$

Perfect azimuthal response is indicated if

$$\frac{R_{\theta, 0}}{R_{\theta, \bar{\phi}}} = \frac{R_{\theta, 30}}{R_{\theta, \bar{\phi}}} = \dots = \frac{R_{\theta, 330}}{R_{\theta, \bar{\phi}}} = 1. \quad (3)$$

Figure 3 through 5 show the azimuthal ratios plotted as a function of azimuth.

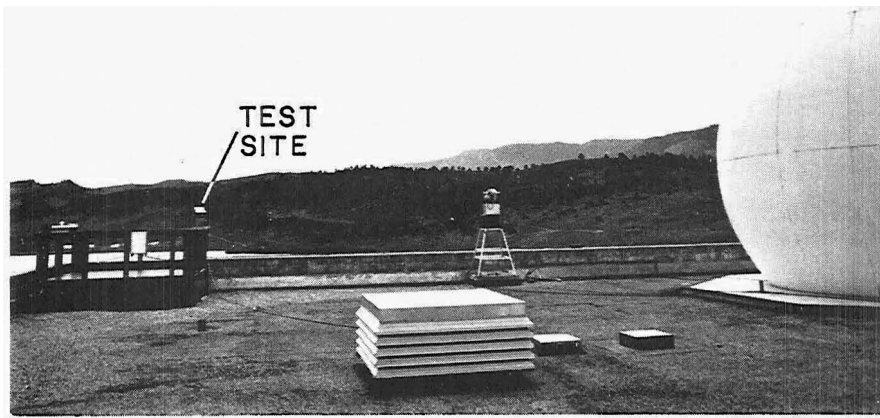


Figure 2. Position of the test site with respect to ground objects.

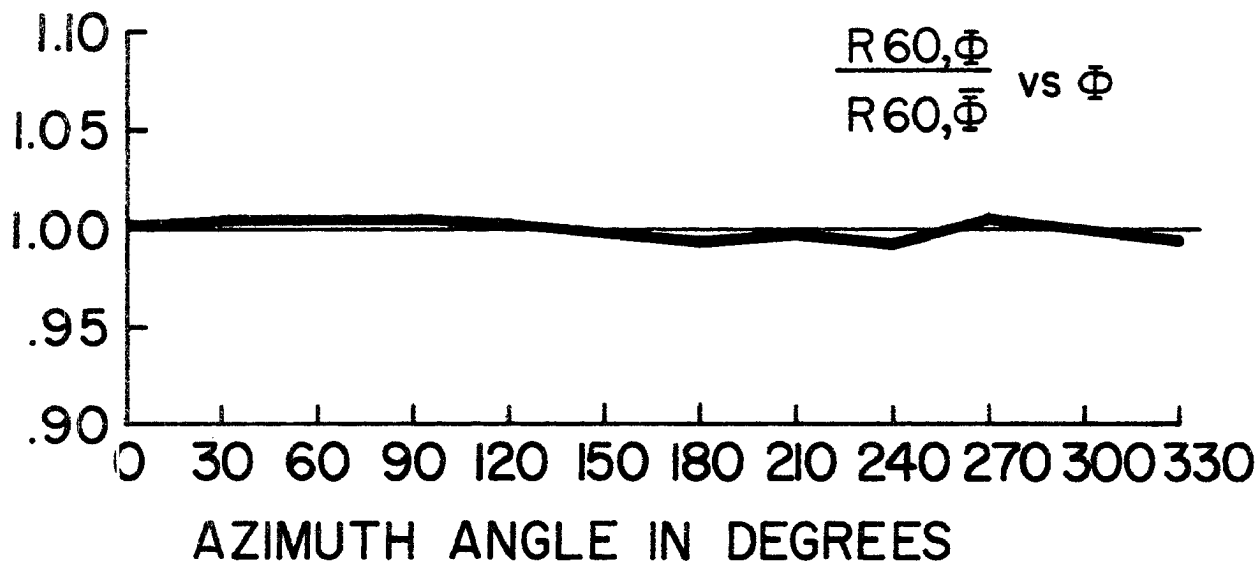
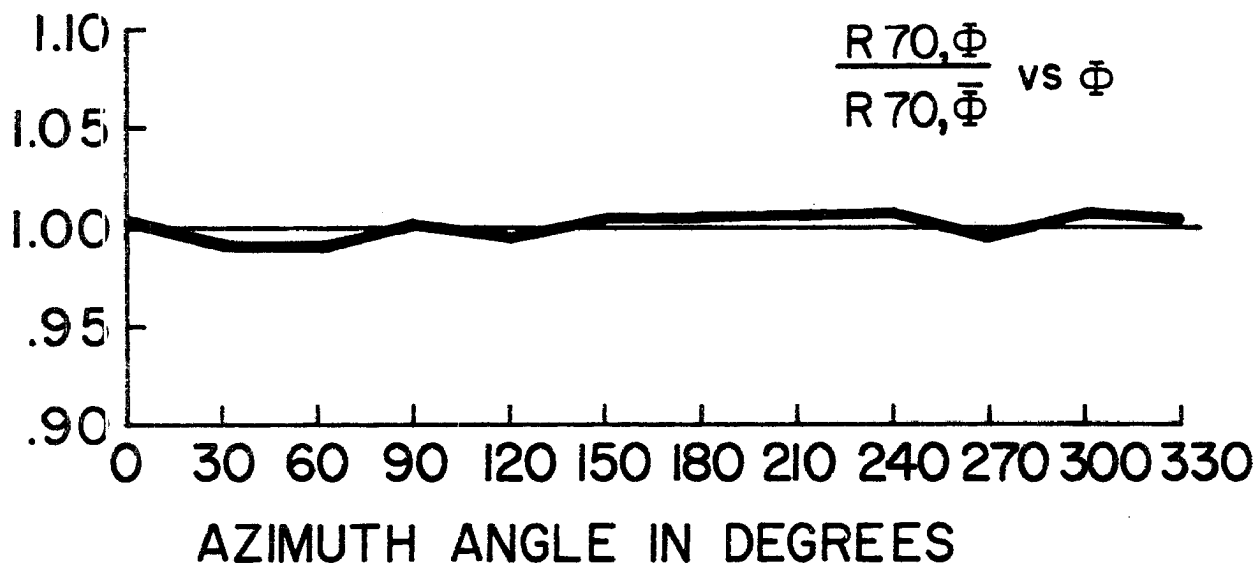
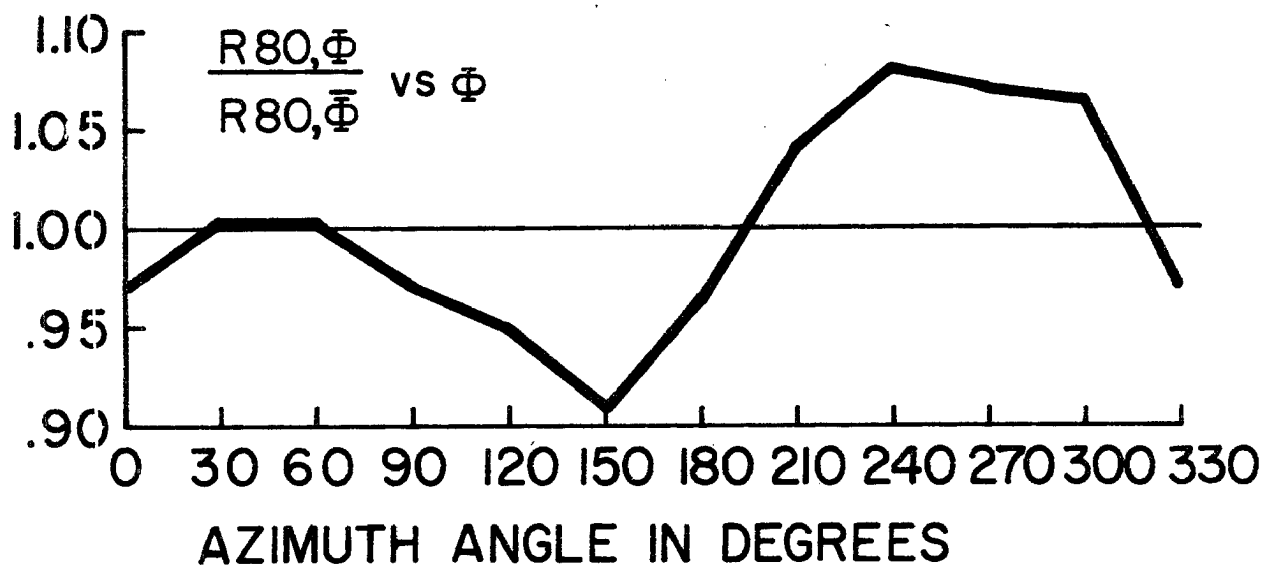


Figure 3. Azimuthal response of the Eppley pyranometer for zenith angles of 80, 70, and 60 degrees.

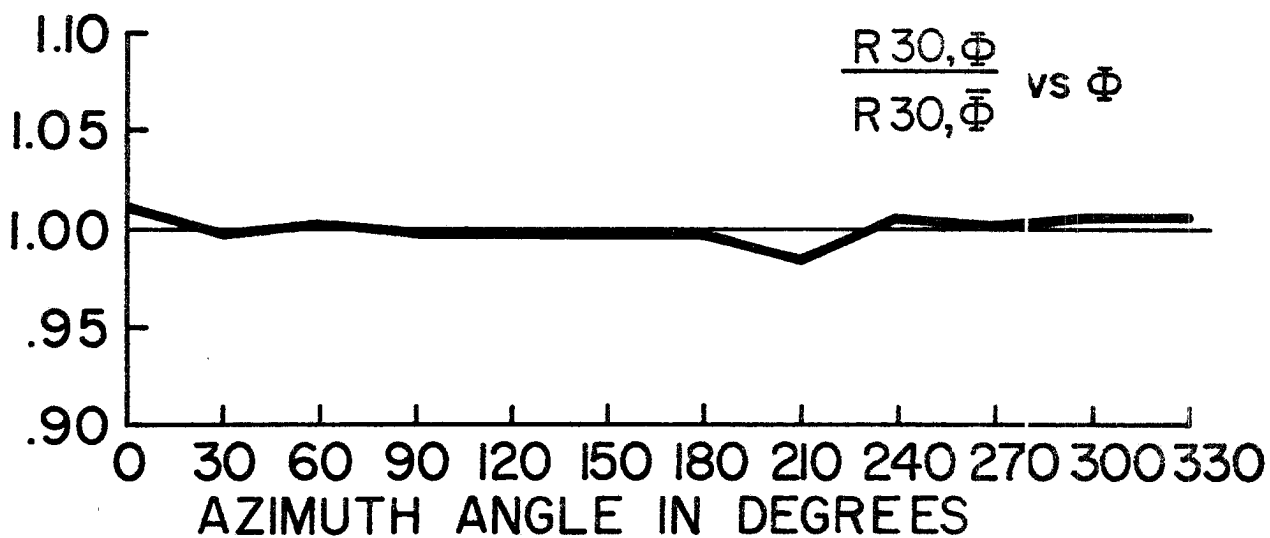
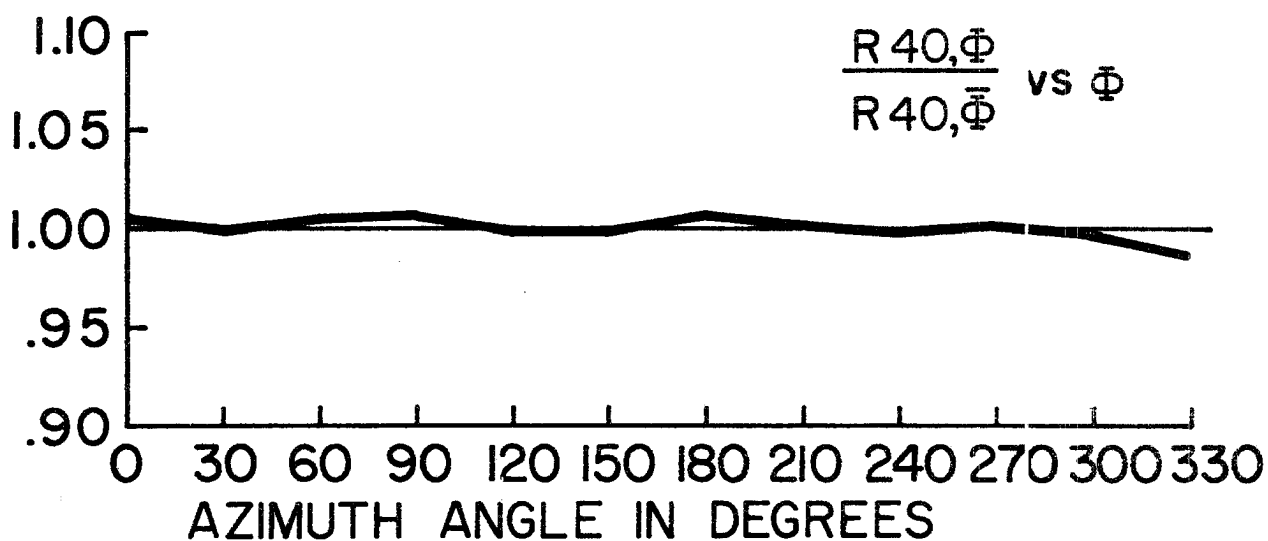
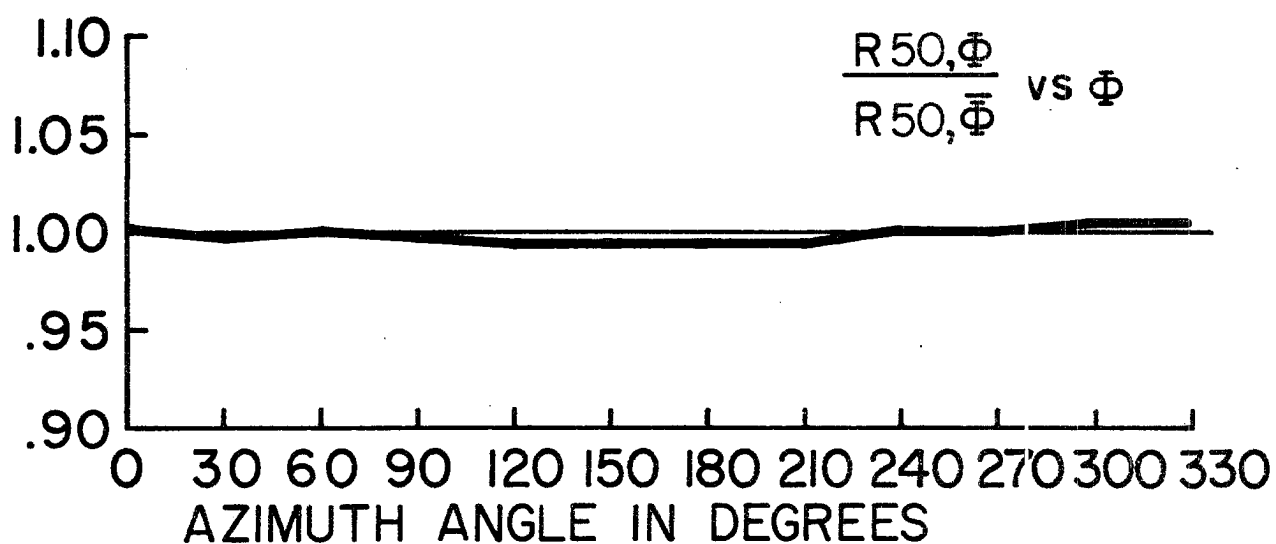


Figure 4. Azimuthal response of the Eppley pyranometer for zenith angles of 50, 40, and 30 degrees.

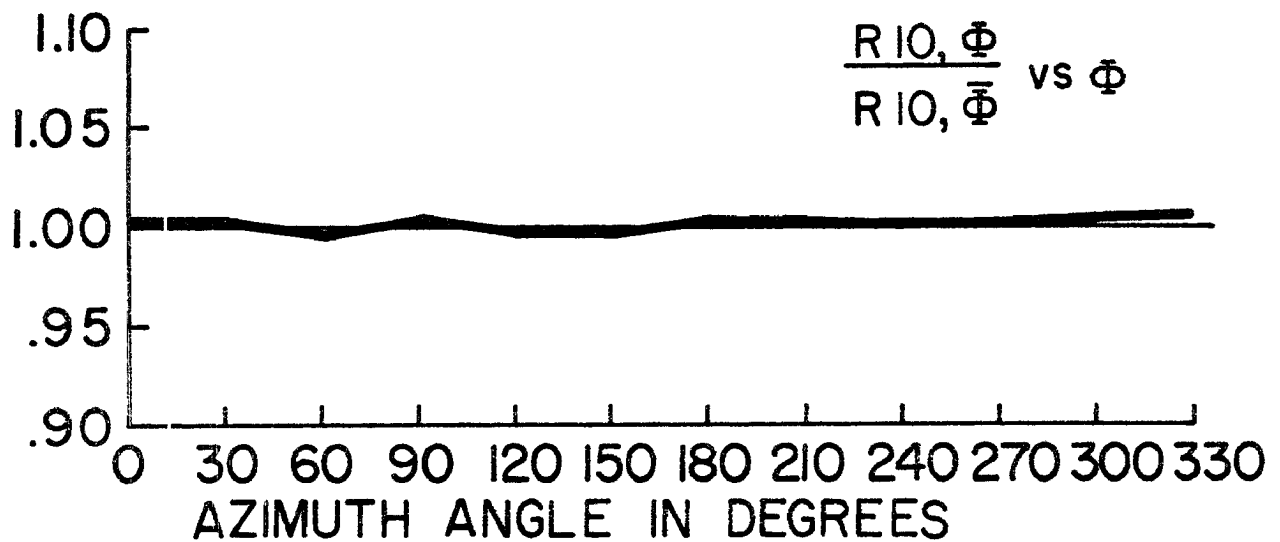
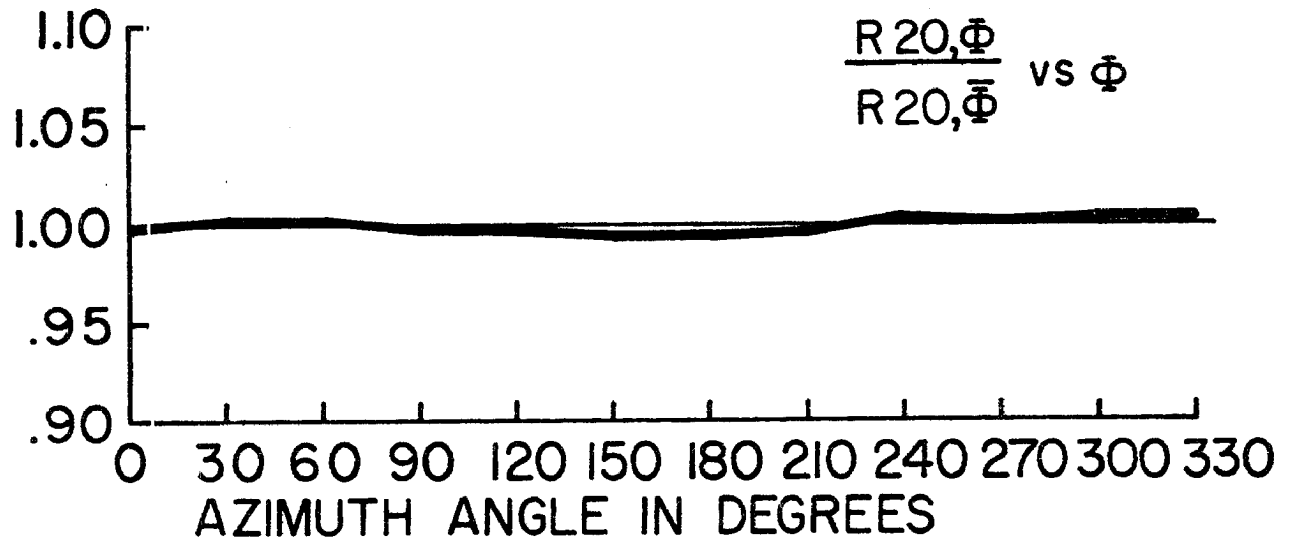


Figure 5. Azimuthal response of the Eppley pyranometer for zenith angles of 20 and 10 degrees.

Figure 6 shows a plot of the ratio $\frac{R_{\theta} \bar{\phi}}{\cos \theta} / \frac{R_{10} \bar{\phi}^*}{\cos 10}$ versus θ . The test of the Eppley instrument was conducted on July 9, 1975 under a nearly clear sky.

* As mentioned previously, the $\theta = 0^\circ$ data is missing. Since R_0 ,
 $\bar{\phi} \approx \frac{R_{10} \bar{\phi}}{\cos 10}$, no significant error should result by using this ratio.

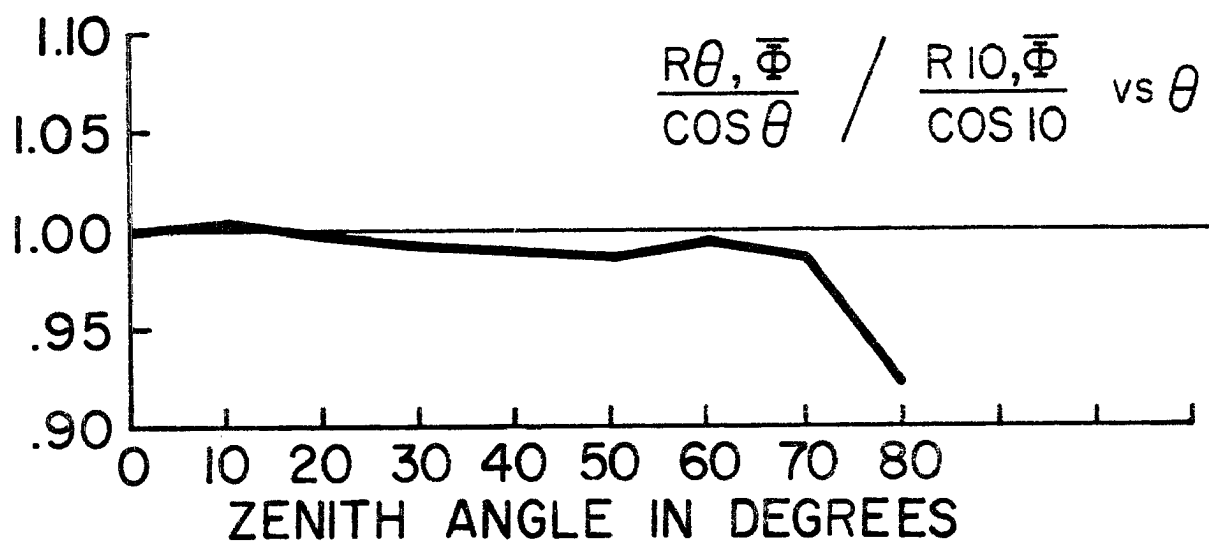


Figure 6. Cosine response of the Eppley pyranometer.

2.4 - TEST OF THE LAMBDA PYRANOMETER

The Lambda pyranometer (serial number PY329-7412), was tested on July 16, 1975 from 11:55 to 12:20 solar time. The cloud cover was somewhat heavier for this test than for the Eppley instrument. The test was carried out in a completely analagous manner to that of the Eppley and the results are displayed in similar fashion in Figs. 7 through 10. All notation carries over from the previous figures. The data for $\theta = 30^{\circ}$ is questionable and incomplete due to a poor electrical connection. Also, the data for $R_{0, 330}$ are missing.

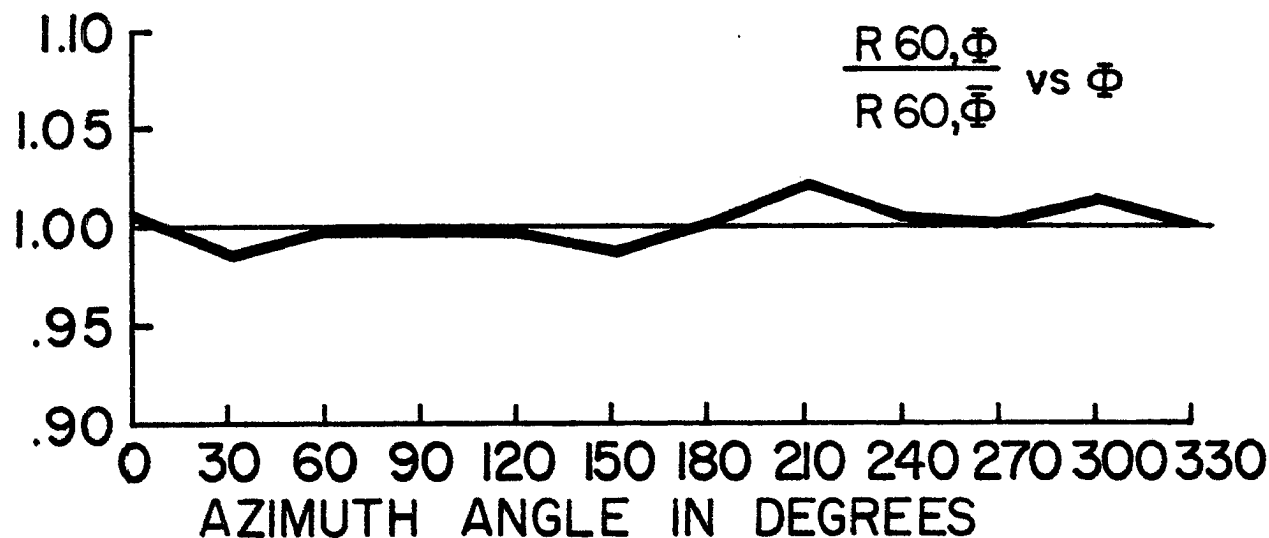
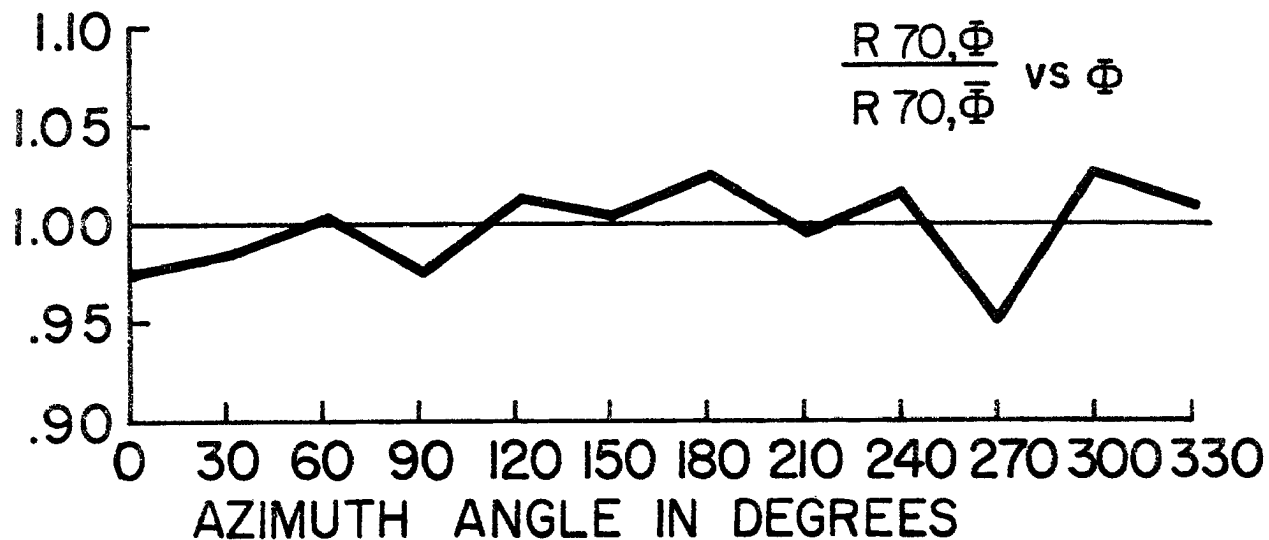
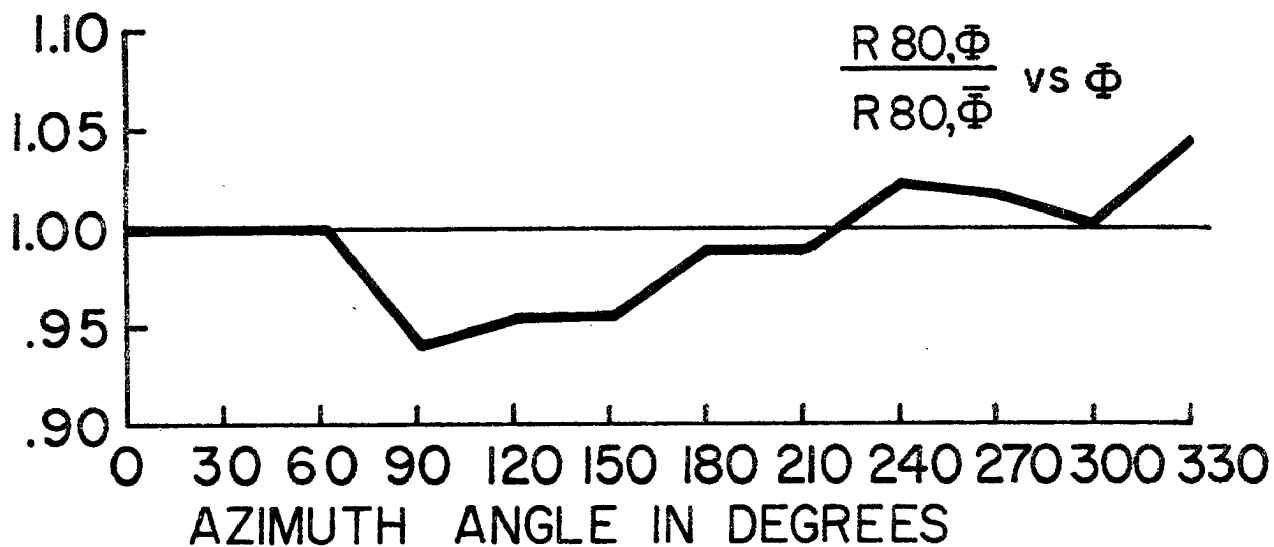


Figure 7. Azimuthal response of the Lambda pyranometer for zenith angles of 80, 70, and 60 degrees.

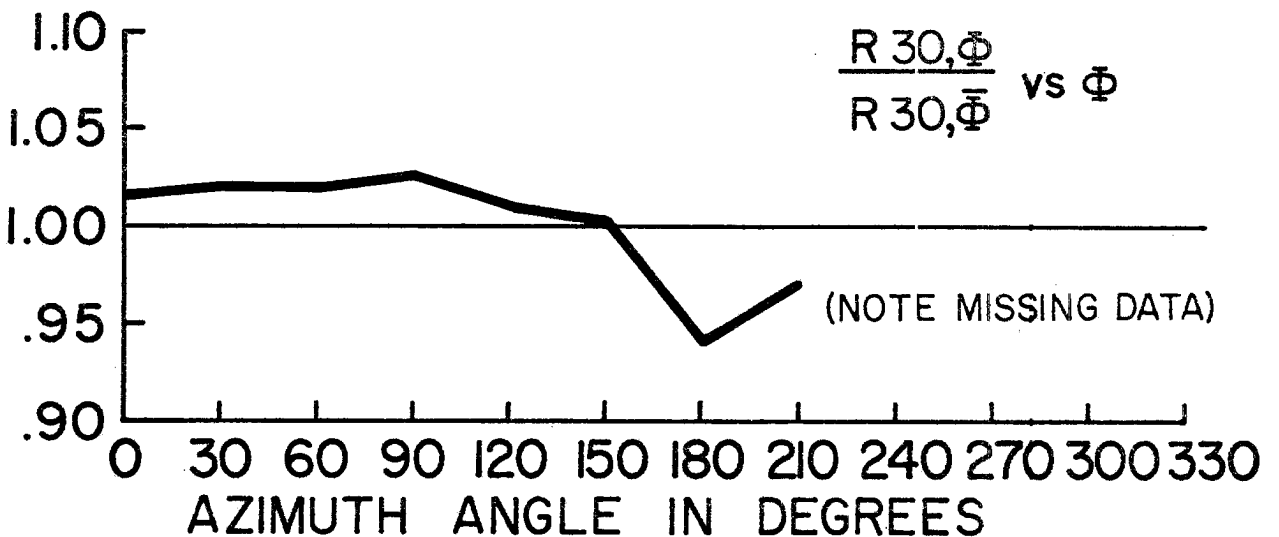
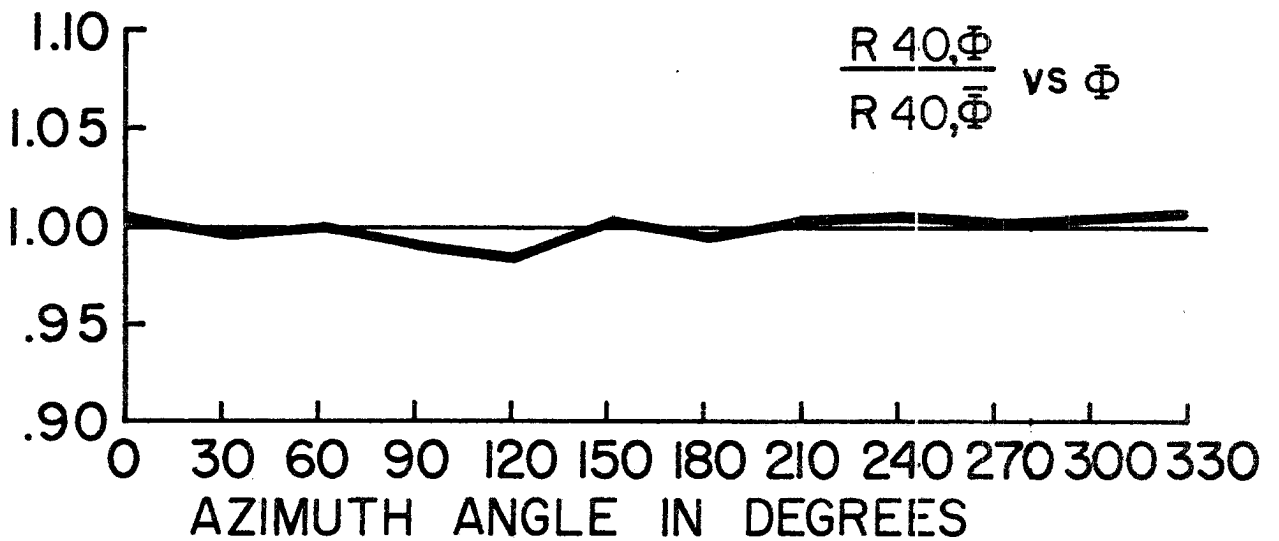
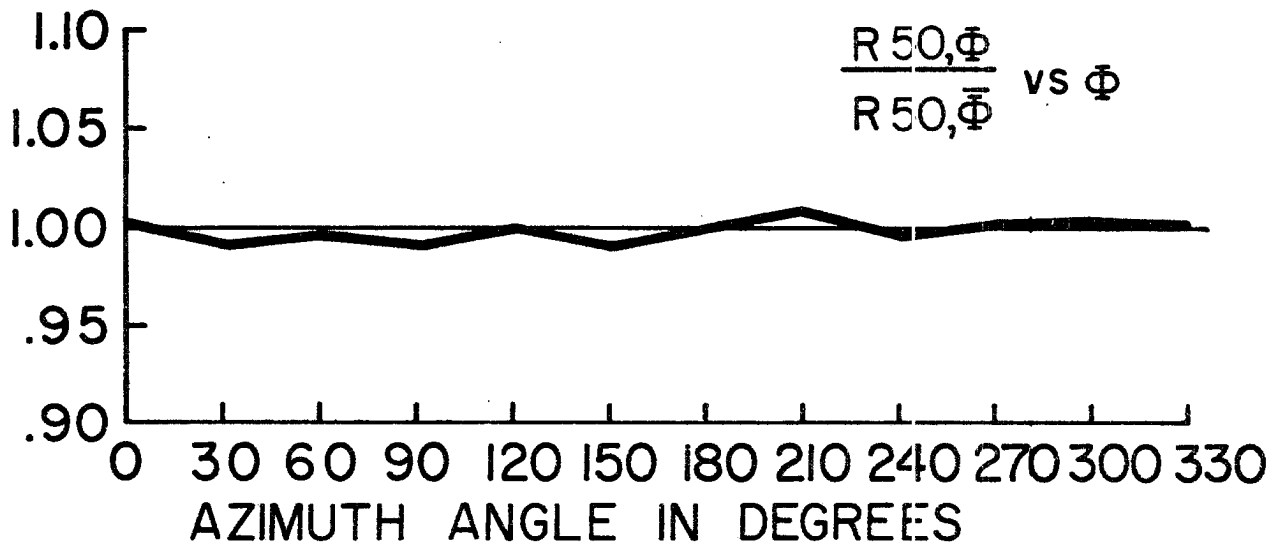


Figure 8. Azimuthal response of the Lambda pyranometer for zenith angles of 50, 40, and 30 degrees.

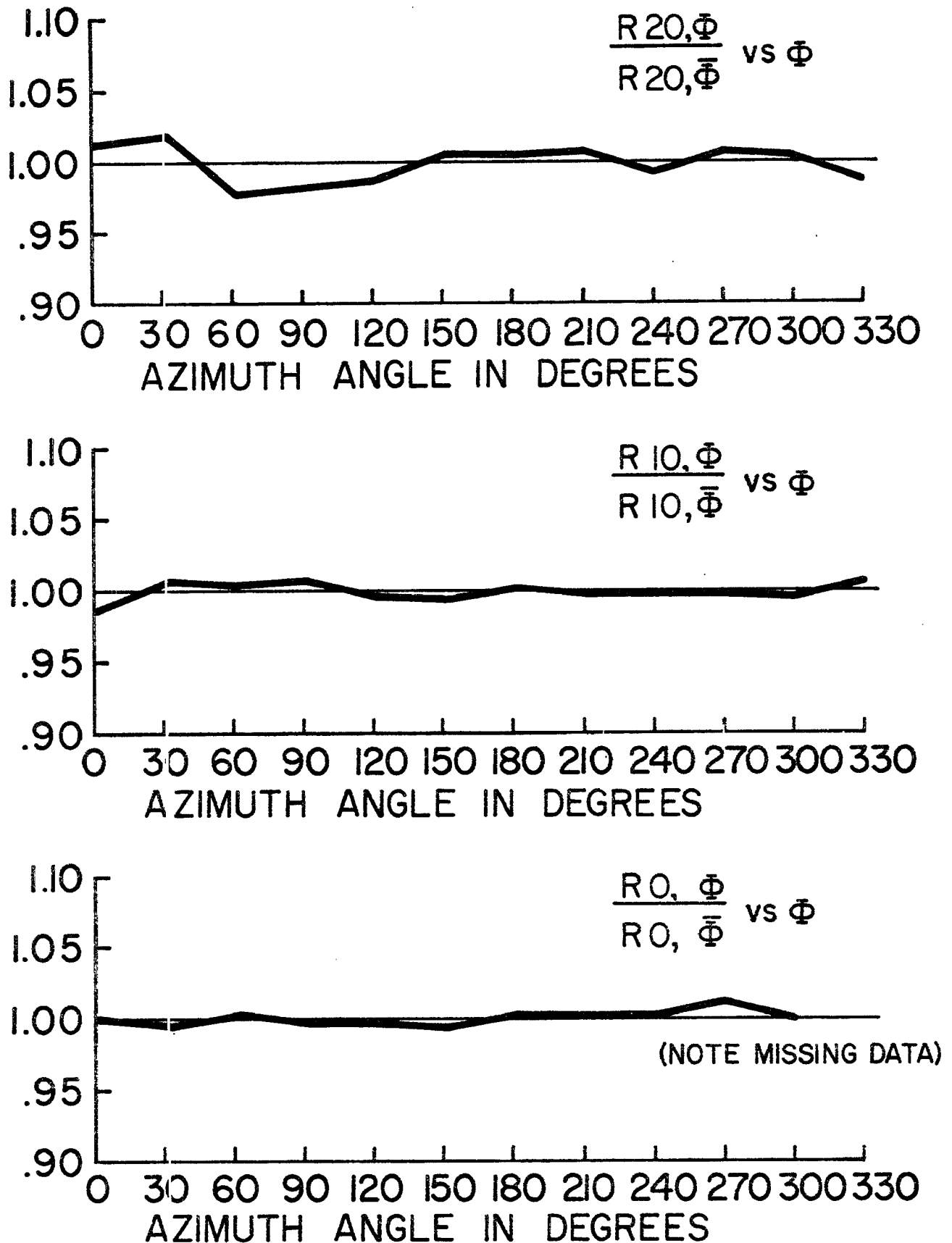


Figure 9. Azimuthal response of the Lambda pyranometer for zenith angles of 20, 10, and 0 degrees.

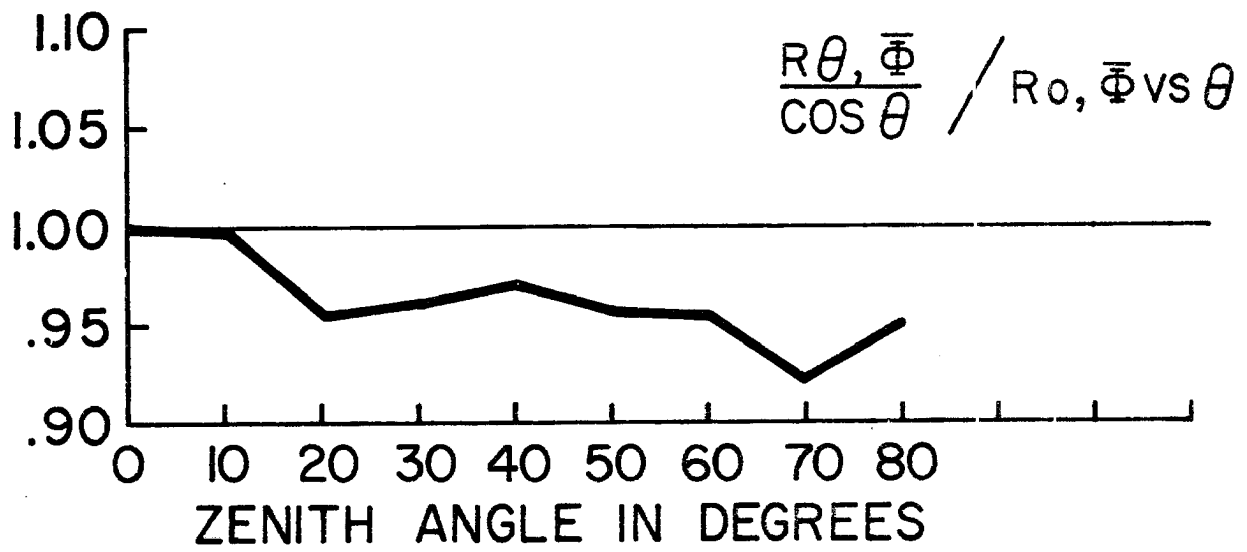


Figure 10. Cosine response of the Lambda pyranometer.

2.5 - SOURCES OF ERROR

Deviation from perfect azimuthal response is due to any of several factors. For the Eppley pyranometer, an uneven thermopile surface, variation in response over the thermopile surface or non-homogeneity of the dome material could all contribute to variation in the response. For the Lambda pyranometer, uneven shape of the diffusing surface or non-homogeneity of the same are major sources for uneven response. Variation in response over the solar cell surface is less a factor since the light striking the surface is of a diffuse nature.

Experimental method is also a source of error. Most critical for the azimuthal response is the actual physical construction of the turntable and leveling of the instruments with respect to the platform on the equatorial mount. A small bend in the turntable shaft would introduce considerable error.

Any of the above sources of error would be most effective in introducing an error at large zenith angles. The results confirm this since deviations are greatest for $\theta = 90^\circ$ and decrease with θ . The periodic nature of the response of the Eppley instrument at $\theta = 80^\circ$ can be attributed to improper leveling of the turntable with respect to the platform of the mount, non-homogeneity of the dome material, an uneven thermopile surface, or to a slight bending of the turntable shaft. The latter seems improbable, however, since no such periodicity is present in the corresponding graph for the Lambda pyranometer.

The small variations which are observed in the azimuthal response for small θ may well have resulted from noise signals in the data collection system since no pattern is apparent and since little improvement is seen as θ decreases.

The experimental error should have a much smaller effect on the cosine response curves **since** much of it is random in nature and will average out over all azimuths. Only the changing sky conditions with time and variation of the diffuse radiation with θ are significant in the cosine response data.

2.6 - CORRECTED COSINE RESPONSE

In an effort to minimize the last two mentioned sources of error, another test of both pyranometers was conducted on August 4, 1975, with some cloud cover again present over the western portion of the sky. At each zenith only two azimuth readings were taken, 180° apart, resulting in about half the execution time needed for the first tests. Also, at each zenith, a diffuse component only reading was taken by shading the instruments from the solar disc. It was hoped in this way to eliminate the dependence of diffuse radiation on changes in zenith. The data obtained in this manner are displayed in Figs. 11 and 12. The trace labeled "corrected" applies to data from which the zenith dependence of the diffuse component has been excluded. Data designated as "uncorrected" assumes this component to be independent of zenith.

Examination of the graphs indicates that in the case of the Eppley tests, clear-day data is not improved upon by compensating for zenith dependence of the diffuse component. Or alternatively, the variation of the diffuse component at this site, at least, has no appreciable variation with zenith for clear sky conditions. The deterioration of the "uncorrected" trace over that of the previous Eppley test indicates that partial cloudiness tends to act to depress values for large θ in uncorrected data. It should be recalled that the first test of the Eppley pyranometer was carried out under clear sky conditions. This is consistent with the fact that the diffuse component of a moderately cloudy sky is greater than that of a clear sky.

Assuming this is the case, the "corrected" data for the Lambda instrument's pyranometer is taken as the best measurement of cosine response. As is evident, the cosine corrected head actually over-corrects for changing zenith after $\theta = 40^\circ$.

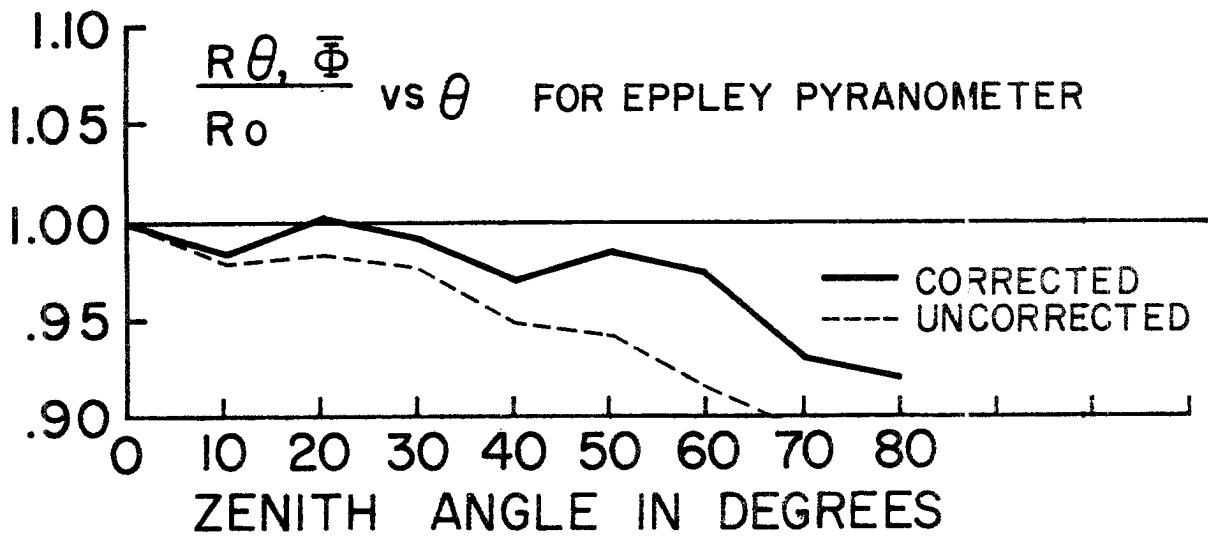


Figure 11. Corrected cosine response for the Eppley pyranometer.

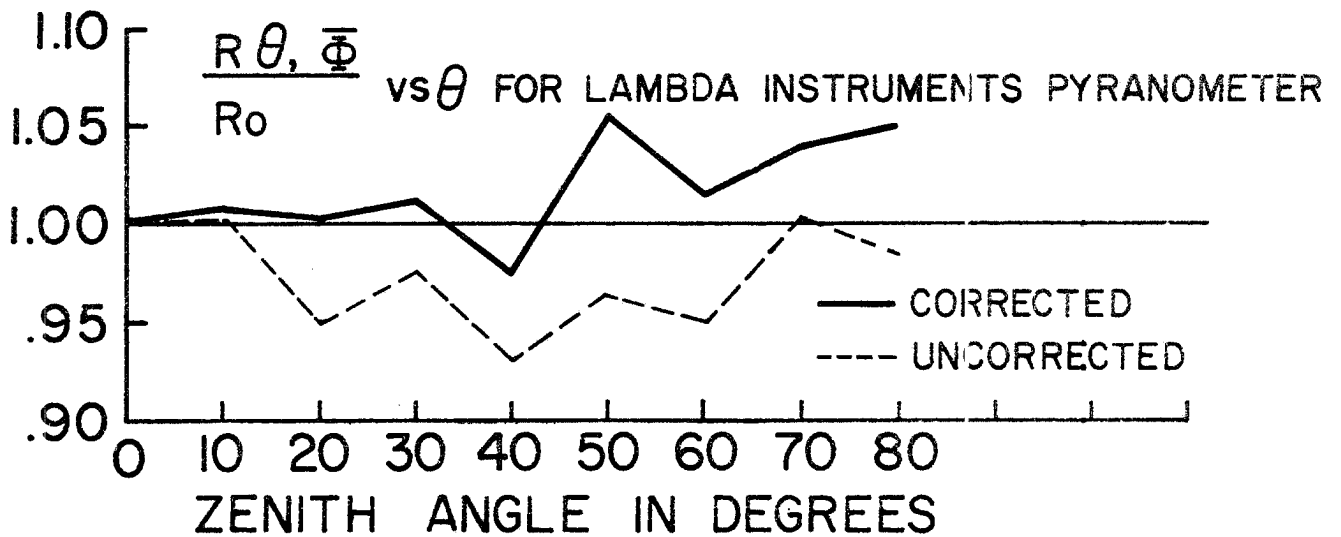


Figure 12. Corrected cosine response of the Lambda pyranometer.

2.7 - COMPARISON OF COSINE RESPONSE WITH THE REGRESSION MODEL

In order to determine if the difference in the cosine response of the two instruments could be detected in the regression coefficients, a simulated cosine response comparison was made. In this comparison the solar altitude dependent regression coefficients were used to generate a projected response for the Eppley instrument, while constraining the Lambda pyranometer to perfect cosine response. Ratios of the relative responses were then taken.

To accomplish this, average solar altitude angles were calculated for day 150, 1975 which corresponded to the intervals I2 through I8 referred to in section I of this report. (Day 150 was selected because of extremely clear morning skies and because data from day 150 was used in the calculation of the regression coefficients.) Assuming a constant direct solar irradiance of 3.6×10^6 joules \cdot meter⁻² \cdot hour⁻¹, appropriate values of a_0 and a_1 (Table 7, Part I) were selected and used in conjunction with the average altitude angles mentioned above, to calculate the response of the Eppley instrument. The parameter a_0 was scaled proportionally greater so it could be used with the high irradiance typical of midday rather than the low post-dawn values from which it was calculated. The effect of this scaling is small. Using the same average solar altitude angles, the constrained response of the Lambda pyranometer was calculated.

In order to compare the regression generated responses to those of the cosine tests, ratios of the relative responses of each instrument were taken. For example, if $\left(\frac{R_\theta}{R_0}\right)_{\text{Lambda}}$ is the relative response of the Lambda pyranometer at zenith angle θ to its value at $\theta = 0^\circ$, values of $\left(\frac{R_\theta}{R_{20^\circ}}\right)_{\text{Lambda}} / \left(\frac{R_\theta}{R_{20^\circ}}\right)_{\text{Eppley}}$ were calculated for both regression and cosine

response data. The value R_{20° was used in both cases in the denominator because this was approximately the smallest average zenith for day 150. Figure 13 shows the comparison. While the cosine response test data shows a greater difference in the instruments, the regression generated curve is seen to follow the same trend. Thus, it can be seen that difference in cosine response is evident in the regression analysis.

It is also consistent that the regression curve yields smaller values than the cosine response curve at large zenith angles. Data from which regression coefficients were calculated was gathered over a number of days. At large zenith angles on a clear day, the over-correction of the Lambda pyranometer would dominate and the regression coefficients should reflect this fact. However, at large zenith angles on partially cloudy days, increased diffuse radiation may tend to suppress this effect, causing a more equivalent output from the two instruments and thus diminishing the difference predicted by the regression model.

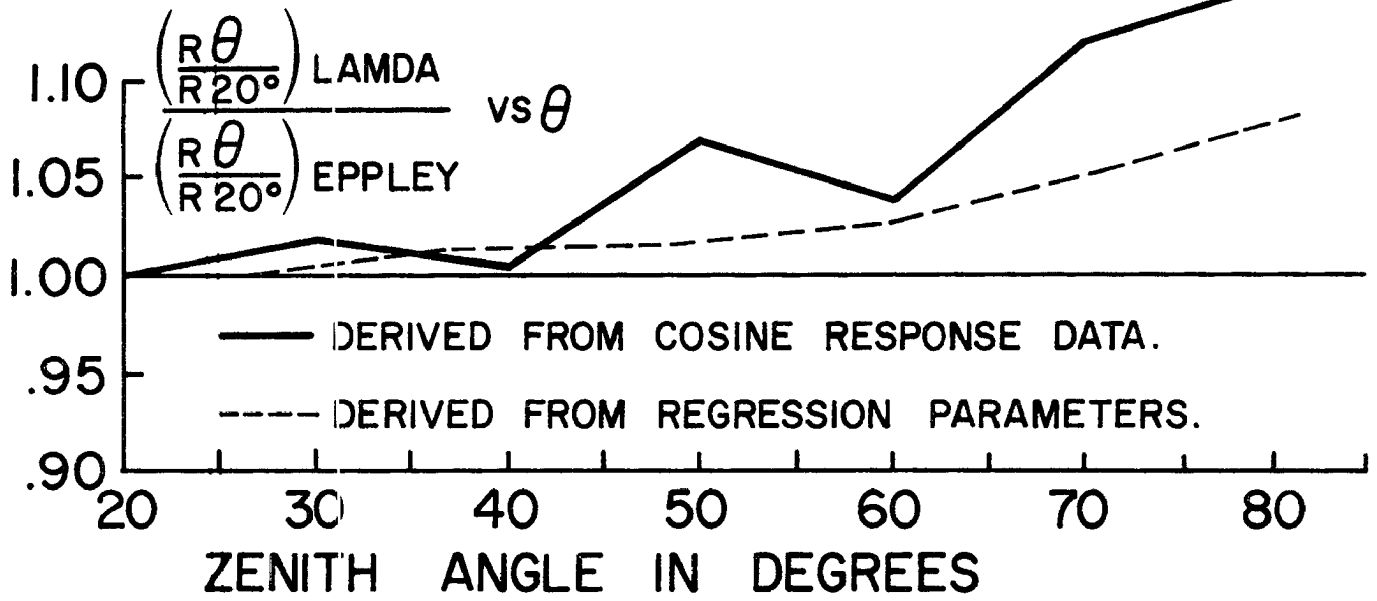


Figure 13. Comparison of cosine response results with linear regression results.

2.8 - CONCLUSION

Both the Eppley and Lambda pyranometers display reasonably good cosine responses. The Eppley domes were found to under-correct for variation of the zenith angle, while the Lambda diffusing head was found to over-correct. No significant trend was observed for either instrument in azimuthal response. The general shape of the compared cosine responses is compatible with the solar altitude dependent regression coefficient.

It should be noted that the cosine response tests are of a relative nature. Each response curve is a measure of the instrument's response at a particular zenith relative to a zenith of 0° . Nothing should be implied about the absolute accuracy of the radiometers from these tests.

REFERENCES

- Jenkins, G. M. and D. G. Watts, 1968: "Spectral Analysis and its Applications". Holden Day.
- Robinson, N., et al, 1966: "Solar Radiation", Elsevier Publishing Co., New York.
- Smithsonian Meteorological Tables, 1966, Sixth Revised Edition.

ACKNOWLEDGEMENTS

The research in this paper was supported by a grant from the Global Atmospheric Research Program, National Science Foundation and the GATE Project Office, NOAA, under grant No. OCD 74-21678.

BIBLIOGRAPHIC DATA SHEET	1. Report No. 250	2.	3. Recipient's Accession No.
4. Title and Subtitle Comparison of a Thermopile Broadband Detector and a Photon Detector for the Measurement of Solar Radiation. Part I. Analysis of Simultaneous Data. Part II. Cosine Response Functions.		5. Report Date April, 1976	6.
7. Author(s) Maria Silva Dias, John Davis, and Stephen K. Cox	8. Performing Organization Repr. No. CSU ATS 250		10. Project/Task/Work Unit No.
9. Performing Organization Name and Address Department of Atmospheric Science Foothills Campus Colorado State University Fort Collins, Colorado 80523		11. Contract/Grant No. N.S.F. OCD 74-21678	
12. Sponsoring Organization Name and Address GATE Project Office NOAA		13. Type of Report & Period Covered	
		14.	
15. Supplementary Notes			
<p>16. Abstracts</p> <p>Solar radiation instruments manufactured by Eppley Laboratories and Lambda Instruments are compared. The primary method of comparison was a detailed inspection of data collected simultaneously from each of the instruments during the summer and autumn of 1975 at Fort Collins, Colorado. Data were stratified both as a function of sky cover and solar zenith angle. In general, hourly and daily insolation values from the two sets of instruments were within 2.5% of one another.</p> <p>Deterioration of the nearly linear relationship between the two instruments occurred at large zenith angles. Results of the investigation of the cosine response of the two pyranometers are presented. The Eppley instrument is characterized by undercorrection for large zenith angles while the Lambda instrument's device over-corrects. The cosine response characteristics are shown to be consistent with the solar-altitude-dependent regression model.</p>			
<p>17. Key Words and Document Analysis. 17a. Descriptors</p> <p>Solar Radiation Measurements Solar Radiation Instruments Pyranometer measurements</p> <p>17b. Identifiers/Open-Ended Terms</p> <p>17c. COSATI Field/Group</p>			
18. Availability Statement		19. Security Class (This Report) UNCLASSIFIED	21. No. of Pages 45
		20. Security Class (This Page) UNCLASSIFIED	22. Price